Reply to review comments

We thank the reviewers for the thoughtful comments, time and efforts spent on reviewing the manuscript. We carefully considered the comments and revised the manuscript accordingly. Below please find our point-by-point replies (colored in blue). Besides, a revised manuscript with tracked changes was uploaded.

Reviewer #1

General comments

The manuscript presents an interesting method to estimate the SO_2 emission rates from volcanic eruptions, based on model simulations and SO_2 index from satellite data. While the paper presents a useful technique which are illustrated with an interesting case study of the Nabro eruption, the description of the method is not clear, in particular how satellite data is used and how uncertainties are addressed, also the results are not sufficiently validated, and references and comparisons to some other key publications on the Nabro event are lacking. The manuscript has potential for publication after being revised, with particular focus on the comments below.

We revised the method description to make the proposed inversion approach better understandable. We also extended the discussion and compared our results with those presented in the suggested key publications. For details please see responses to specific comments below.

Specific comments

1. "Ensemble-simulations":

- The authors refer to the term "ensemble simulations" throughout the manuscript, which is not explained until section 3.1. It needs to be clarified in the very beginning of the paper.

Following other review comments, the term "ensemble simulations" has been removed or rephrased throughout the manuscript in order to avoid unnecessary confusion. The changes are found in the revised manuscript (with tracked changes): page 1, title, page 2, line 9, page 4, line 12, page 5, line 25, page 6, line 4, line 8, line 26, page 11, line 7, page 12, line 4, line 5, page 17, line 22, which correspond to those on page 9103, title, 9104, line 9, page 9106, line 1, page 9107, line 9, line 11, line 15, line 20, page 9111, line 9, page 9112, lines 1-3, page 9117, line 7 in the original GMDD paper.

- In the introduction it is stated that "The fine temporal and spatial discretization of this domain creates a need for large-scale ensemble simulations". This is unclear. First, what is the argument for using a very finely discretized emission domain, and second, why does this create a need for ensemble?

The volcanic emissions in the Nabro case study are strongly time- and altitude-dependent. We discretized the emission domain as finely as technically feasible in order to reveal local details

of the SO_2 emissions at high temporal and spatial resolution. This way, we expect to obtain more reliable simulation results. However, the fine discretization increases demands on computing capabilities. The iterative estimation procedure of the emission rates requires a large number of unit simulations. Besides, a study based on a sufficiently fine discretization can provide us valuable reference information for the further development of an adaptive discretization strategy that may help to reduce the computational burden in future work. To clarify we modified the text on page 9107, lines 6-12 (GMDD paper), which is found on page 5, lines 23-29, page 6, lines 1-5 in the revised manuscript (with tracked changes).

- In section 3.1 the authors finally explain that they refer to the set of all unit simulations in the inversion procedure as an "ensemble simulation". However, is this really characterized as ensemble simulations? Ensemble dispersion modelling implies, as explained by Galmarini et al. (2004) (doi:10.1016/j.atmosenv.2004.05.030), variations in the meteorological drivers and/or source parameters, or the approach to dispersion modelling by using different models. I do not see that these simulations fall under either of these categories. They are simply "sensitivity"-simulations, "scenario"-simulations, "unit"-simulations, or sometimes described as "source-receptor" relationships. I do not see how they are true ensemble simulations. Please justify the use of this term, or consider changing to another wording.

We agree and removed or rephrased the term "ensemble simulations" used for describing our inversion approach. Please see reply to comment 1. "Ensemble-simulations".

2. Methodology description (Section 3):

It was sometimes quite hard to follow and understand the methodology, mainly the first section 3.1. In particular I did not fully understand

- the difference or similarity between the terms "ensemble simulations" , "forward simulations" and "model forecasts", which seem to be used interchangeably? Also, in the abstract you point out two types of simulations; "ensemble", and "final transport simulations". A more consistent wording is needed throughout the paper.

Following earlier comments we made corresponding changes regarding the term "ensemble simulations". For consistency, we replaced the term "final transport simulations" on page 9104, line 10, line 21, page 9111, line 13, page 9112, lines 14-15, line 25 (GMDD paper) with "final forward simulations" on page 2, line 10, line 21, page 11, lines 18-19, page 12, line 25, page 13, lines 6-7 in the revised manuscript (with tracked changes). The term "model forecasts" refers to the results of the "final forward simulations".

- the justification for using 12 h accumulated model and observations data?

The AIRS instrument requires 12 h to gather observations on a global scale. At mid and low latitudes there are typically two satellite overpasses per day (at 01:30 and 13:30 local time). An accumulation time interval shorter than 12 h may lead to time periods in the CSI analysis during which the satellite observations do not cover the volcanic plume at all. Therefore 12 h is a reasonable minimum time period for this analysis. To clarify we added text on page 13, lines 16-20 in the revised manuscript (with tracked changes).

- why the importance weights need to be estimated iteratively? You say this is needed in order to obtain reliable results, please elaborate. Why do the unit simulations have to be re-run for each iteration (alas section 4.1)?

As an initial guess for the first iteration, the simulated air parcels are distributed uniformly in the considered time- and altitude-dependent initialization domain. Correspondingly, the importance weights for all 15840 subdomains are 1/15840. In order to find more realistic importance weights that reflect the relative distribution of emissions in the subdomains, unit simulations then have to be performed to estimate importance weights in an iterative scheme. Changes in the importance weights indicate how many air parcels should be reassigned to each subdomain and considered as new initial conditions for the next iteration.

In our case, after 1-2 iterations we already obtained rather stable importance weights that led to good simulation results. Nevertheless, in order to establish a robust computational procedure, we defined a stopping criterion for the iterative update process. Namely, the iterative procedure will stop when the change of the updated importance weights is sufficiently small. Here, the change of the importance weights is evaluated according to a given mathematical measure that is based on the Frobenius norm. In this study, by choosing a threshold of 1% for the relative difference of the updated important weights, the stopping condition was fulfilled after 3 iterations (see page 16, lines 16-17 in the revised manuscript with tracked changes).

To clarify we added text on page 12, lines 15-22 in the revised manuscript (with tracked changes).

- In section 1 it is stated that the algorithm does not require explicit source-receptor relationships. But this is not clarified any further in the methodology section. Please explain.

By saying source-receptor relationships we mean the full source-receptor matrix computed based on the forward model and the discretization of the unknown quantity on a regular grid (cf. Seibert (2000) and related works), which is used for the solution of the arising linear inverse problem. In our approach this source-receptor matrix is not explicitly calculated. More details have been addressed on page 9106, lines 18-27 in the GMDD paper.

- what is “new” compared to the methods by Stohl et al (2011) and Flemming and Innes (2013), and what are the benefits of your method compared to those previously published methods? This should be clearly stated already in the Introduction.

In the work of Stohl et al. (2011) and Flemming and Inness (2013), the forward models FLEXPART and ECMWF’s IFS were applied, respectively. In this study, we used our recently developed Lagrangian transport model Massive-Parallel Trajectory Calculations (MPTRAC) to perform forward simulations at large scale. The work of Stohl et al. (2011) extended the inversion algorithm initially presented in Seibert (2000). Compared to that approach our inversion approach requires no a-priori information on the emissions and does

not require the calculation of the full source-receptor matrix. Compared to the work of Flemming and Inness (2013), we considered a much finer discretization for the unknown time- and altitude-dependent emission function (250 m in altitude and 1 h in time in our case, about 2–3 km and more than 6 h in the case of Flemming and Inness (2013), and 19 vertical layers stacked up to 12.3 km altitude and 3 h time intervals in the case of Stohl et al. (2011)). We did not find a need to solve the ill-posed inverse problem by means of a Tikhonov or smoothing constraint. Furthermore, the Critical Success Index (CSI) was used here for the first time to evaluate the goodness-of-fit of the forward simulations and to estimate the importance weights of the time- and altitude-dependent SO_2 emission distribution. This way, we were able to provide relative distributions of the emissions in a two-dimensional view (in time and altitude) and its local details at relatively high (or even unprecedented) temporal and spatial resolution.

We modified the text on page 9107, lines 12-15 (GMDD paper) that emphasizes the advantages of our inversion approach. Improved text can be found on page 6, lines 9-21 in the revised manuscript (with tracked changes).

3. Adequate referencing:

The authors should refer to and compare their results to the following two publications which also reported on SO_2-inversions and satellite-derived height estimates for the Nabro eruption:

- Theys et al. (2013) Volcanic SO_2 fluxes derived from satellite data: a survey using OMI , GOME-2 , IASI and MODIS, Atmospheric Chemistry and Physics, doi:10.5194/acp-13-5945-2013.
- Clarisse, L. et al. (2014) The 2011 Nabro eruption, a SO_2 plume height analysis using IASI measurements, Atmos. Chem. Phys., 14, 3095-3111, doi:10.5194/acp-14-3095-2014

We added these two references in the introduction section on page 4, lines 21-22 in the revised manuscript (with tracked changes). We also discussed and compared the results from these two publications and our work in the revised manuscript. We improved the text in the introduction, in Sect. 2.3 (validation data sets), in Sect. 4.5 (validation of emission time series) and in Sect. 4.6 (final forward simulations), accordingly.

4. Altitude sensitivity:

How is averaging kernels handled in your approach (see explanations and Figure 1 of the above mentioned Theys et al. (2013) paper)? You say in section 2.2 that the AIRS SI is most sensitive to SO_2 layers at about 8 to 13 km altitude which reflects the infra-red kernel. Do you take this altitude-sensitivity into account when you compare model and observation data? I.e. do you count the model values below 8 km in the same way as those above 8 km, or are they weighted by the averaging kernel so that low altitude model values count less since the satellite data is less sensitive at these heights? In other words, the AIRS SI data might not contain information to constrain the emissions below 3-5 km altitude. How do you deal with this?

The SO_2 kernel functions of the AIRS channels used to calculate the SI depend on atmospheric conditions and altitude (e.g., Hoffmann et al. (2016, Fig. 1)). However, variations

in the UT/LS region where most of the Nabro emissions occurred are not too large. Hence, we did not consider this dependency in our analysis. However, the consideration of the AIRS kernel functions in the CSI analysis will be an important aspect in future work.

To clarify we added the aforementioned text to the Outlook section on page 26, lines 26-29, page 27, lines 1-2 in the revised manuscript (with tracked changes).

5. Uncertainties:

How do you deal with uncertainties in the satellite SI index, and also uncertainties related to the unit simulations in particular to errors in the meteorological driving data? At longer forecast times it is likely that the errors in the meteorological data are more important.

Uncertainties in the meteorological data are an important source of error. The topic is addressed in a recent study by Hoffmann et al. (2016), wherein four different meteorological products have been tested for the MPTRAC simulations. The study shows that spatial and temporal resolution of the meteorological data is an important factor influencing the quality of the simulations. Here we used the ERA-Interim reanalysis, which provides good accuracy for the simulations. Better results were only obtained with ECMWF operational analysis, which poses higher demands regarding the memory available on the computing system. This work aims to introduce an inversion for SO_2 transport simulations. A more detailed, quantitative study of the errors resulting from the uncertainties of different meteorological data will be considered in future work. To clarify we added the aforementioned text to the outlook on page 27, lines 2-7 in the revised manuscript (with tracked changes).

We also added more detailed information on the measurement uncertainties of the AIRS SO_2 index on page 9, lines 12-13 in the revised manuscript (with tracked changes). The precision of the SI is quite good (0.14 K at 250 K scene temperature) and we concluded that measurement noise has only minor effects on the inversion results presented here.

6. Loss of SO_2:

Do the MPTRAC SO_2 simulations take into account decay of SO_2 by for example reaction with OH? This would be important particularly on the >2 days time scales.

The version of MPTRAC used in this study does not consider any loss processes of SO_2. Hoffmann et al. (2016) considered a newer version of MPTRAC, which takes into account chemical decomposition of SO_2 based on a simple exponential decay model. Our analysis reveals that the simulation results by means of the two different versions of MPTRAC are rather similar. In particular, the relative distributions and patterns of the SO_2 plume remain the same. Only the total amount of SO_2 is changing slowly over time. Note that typical e-folding lifetimes of SO_2 in the UT/LS region are about 7-14 days, which is about the entire time period covered by the simulations.

7. "Validation":

The authors refer in several places to validation of their algorithm by comparisons to the AIRS satellite observations. However, this is not an independent set of data since these data

were used to reconstruct the altitude-dependent SO_2 emission time series. This should be highlighted, and perhaps a better word is "evaluate". A better and independent dataset for validation would be IASI. In the above mentioned two papers (Theys et al (2013) and Clarisse et al (2014) there are many sources of data which you could use for validation. I consider this aspect the most important which needs extensive improvements. A thoughtful validation in lines with that presented in Theys et al. (2013) and Clarisse et al. (2014) is needed.

To extend the discussion we added in Sect. 4.6 in the revised paper: "*Our simulation by means of the product rule and AIRS satellite observations yields similar relative horizontal distributions of SO_2 on 15 June 2011 compared with IASI satellite data and FLEXPART model output as reported by Theys et al. (2013, Fig. 10a). Simulation results for other days, e.g., for 16, 18 and 20 June 2011 are also similar to the GOME-2 satellite retrievals reported by Theys et al. (2013, Fig. 10b – Fig. 10d). Our simulations (Fig. 12 and Fig. 14) show more realistic transport patterns on 14 and 16 June 2011 than the FLEXPART model outputs based on the IASI data (Theys et al., 2013, Fig. 12). Besides, the SO_2 distributions on 16 June 2011 and 18 June 2011 in China are not well captured by the FLEXPART model outputs based on the GOME-2 data (Theys et al., 2013, Fig. 10b and Fig. 10c), but by our simulations (Fig. 14 and Fig. 15). Furthermore, the SO2 transport patterns of our simulations are in good agreement with IASI observations that were extensively studied in the context of the Nabro eruption (Clarisse et al., 2014, Figs. 6–10).*"

Compared to the work of Theys et al. (2013, Fig. 12), we got the impression that our simulation may actually show even more realistic transport patterns, in particular on 14 June and 16 June, see figures below (left: AIRS observations, right: MPTRAC simulation results). However, this finding is based on visual inspection rather than a quantitative comparison.

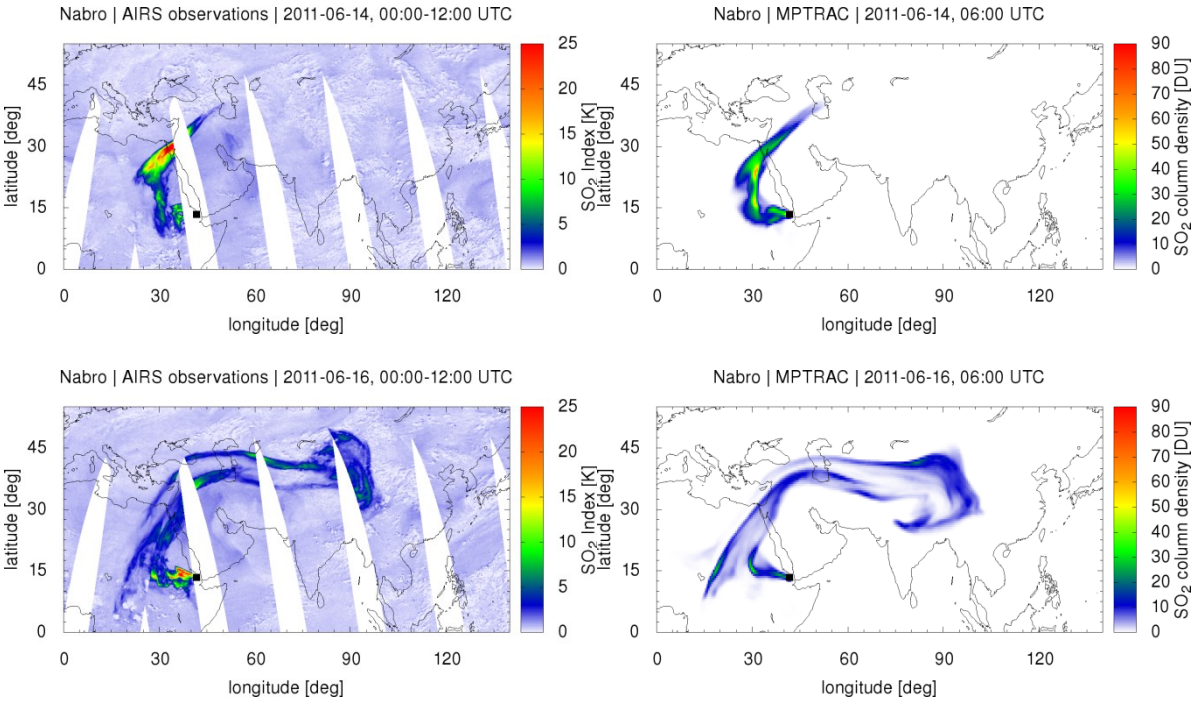

To further validate the reconstructed SO_2 emissions, we added the following text on page 23, lines 19-21 in the revised manuscript (with tracked changes): "*Clarisse et al. (2014) also*

reported that the early Nabro plume mostly raised to altitudes between 15 and 17 km, which agrees well with our reconstructed emission time series (cf. Fig. 5).". We also added text in Sect. 4.6*: "Furthermore, the SO_2 transport patterns of our simulations are in good agreement with IASI observations that were extensively studied in the context of the Nabro eruption (Clarisse et al. (2014), Figs. 6 –10).*"

We updated Fig. 11-17 in the revised manuscript by showing results for 13-16 June, 18 June, 20 June and 24 June) in order to allow for a direct comparison with the results presented by Theys et al (2013). We also added a brief introduction and overview of GOME-2 and IASI satellite measurements to Sect. 2.3 (validation data sets) in the revised paper.

8. Resolution:

In Section 4.1 you specify that you use a 1 h time step and 250 m altitude step leading to 15 840 emission domains. You do not specify how much AIRS satellite data you have, the temporal resolution and number of SI values. Do the AIRS satellite data contain enough information to constrain the emissions at this high resolution? Would the emission subdomain at 16.25 km altitude be sufficiently different from 16.5 km altitude? This also relates to the resolution of the meteorological data (both vertically, and the 3-6 hourly temporal resolution) you used for the unit simulations. Please elaborate

In this study, we tried to discretize the emission domain as finely as possible as permitted by the computing resources. This way, it is possible to reveal more local details of the emissions in case that high resolved meteorological and satellite data are available. It can also provide us information for the further development of an adaptive strategy for discretizing the emission domain, which will be considered in future work. During the time period 12 to 18 June AIRS detected volcanic SO_2 in nearly 75.000 satellite footprints, which means that the inversion is constrained by a large number of individual satellite observations. We added text on page 17 lines 14-16 in the revised manuscript (with tracked changes): "*During this time period AIRS detected volcanic SO_2 in nearly 75.000 satellite footprints. Hence, the inversion of volcanic SO_2 emissions is constrained by a large number of satellite observations.*"

9. Section 4.3:

It is not clear to me how you obtain 0.1052 kg m^{-1} s^{-1} as the equal emission rate. Since you are using "binary" satellite data, i.e. the SO_2 index data, how does the inversion itself produce quantitative emission rates? Or are you distributing the 1.5x10*9 kg estimate from Clarisse et al 2012 over the entire emission domain? In that case I get 1.2e9 kg / (475200 sec*30000 m) = 0.0842 $kgm^{-1}s^{-1}$. Also later you say "since the total amount of emitted SO_2 is fixed" while this is not stated before. Please clarify.

The method does not provide an estimate of the total amount of SO_2 released, but tries to optimize its relative distributions in height and time. The manuscript was revised to make this more clear.

If we distribute the 1.5×10^9 kg total mass estimate from Clarisse et al. (2012) over the entire emission domain, the emission rate by assuming air parcels are equally distributed over the domain is 1.5×10^9 kg / (475200 sec × 30000 m) ≈ 0.1052 kg m^{-1} s^{-1}.

10. Section 4.4:

You should highlight that the comparison of the SO_2 emission rates with the aerosol observations (e.g. CALIOP) is not a direct comparison as one is gas and the other aerosol which would be either sulfate (converted from the SO_2) or ash. In Clarisse et al. (2014) this is nicely explained.

For the evaluation of the SO_2 heights we used MIPAS and CALIOP H_2SO_4 (sulfate aerosol) detections. This aerosol forms from the SO_2 and hence, it can be seen as an indicator for the position of the SO_2. As other studies already found (Fromm et al., 2014; Clarisse et al., 2014) there was very little ash in the Nabro plume. However, to really make sure that we did not compare with ash, we checked the CALIOP depolarisation ratio (no depolarisation for liquid particles) and filtered out volcanic ash using the MIPAS volcanic ash detection algorithm (Griessbach et al., 2014).

To clarify this we added text in Sect. 4.5 (validation of emission time series) on page 22, line 28, page 23, lines 1-6 in the revised manuscript (with tracked changes).

Reviewer #2

Overview:

The paper describes a method to construct emission height and rate of SO_2 emitted from volcanic eruptions. The method juxtaposes large-scale ensemble simulations of a lagrangigan trajectory model and satellite retrieved SO_2 indizies (AIRS) to obtain these parameters in an iterative way. The method is applied to the 2011 Nabro eruption. The final forward model simulation using these parameters is evaluated with AIRS SO_2 and compared with imagery from MVIRI IR and WV and aerosol profiles from CALIPO and MIPAS.

General remarks:

Estimating volcanic emissions from satellite retrievals of ash or SO_2 is an important scientific task. The estimates are usually rather uncertain because of the limitations of the satellite retrievals and uncertainties in the transport simulation. Different approaches have been applied in the past and the one presented in this paper might be an interesting new approach.

However, the paper in its present form cannot convince the reader of the merits of the method and, more importantly, the validity of the results because of the following main points.

We carefully revised the manuscript according to your specific suggestions below.

(i) A major omission is that the results (emission parameters) are not compared with other studies presenting SO_2 emission (flux and height) estimate for the Nabro such as Theys et al. (2013).

We added two more references (Theys et al., 2013; Clarisse et al., 2014) in the introduction section to address their contributions to the study of the Nabro volcanic eruption. Discussions

on the comparison of the SO_2 inversions and satellite/derived height estimates have been added and can also be found in our responses to the comments of Reviewer 1 (7. Validation). Correspondingly, we revised the introduction section and discussions in Sect. 2.3, Sect. 4.5 and Sect. 4.6 in the revised manuscript.

(ii) Although SO_2 and ash plumes sometimes coincide, but they do often not so. The evaluation of the SO_2 emission heights with aerosol retrievals (CALIPO and MIPAS) as well as the imagery is therefore questionable. Another SO_2 retrieval (IASI, GOME-2, OMI) would have been the best choice for the validation of the results with independent observations.

We extended the discussion and compared our results with the work of Theys et al. (2013) and Clarisse et al. (2014), which provide extensive studies of SO_2 retrievals and inverse modeling based on nadir satellite instruments such as IASI and GOME-2.

The main motivation for a comparison with CALIOP and MIPAS is that these instruments provide accurate altitude information due to their measurement geometries (lidar and limb sounding), which is not directly provided by the nadir instruments. For the evaluation of the SO_2 heights we used MIPAS and CALIOP H_2SO_4 (sulfate aerosol) detections. This aerosol forms from the SO_2 and hence, it can be seen as an indicator for the position of the SO_2. As other studies already found (Fromm et al., 2014; Clarisse et al., 2014) there was very little ash in the Nabro plume. However, to really make sure that we did not compare with ash, we checked the CALIOP depolarisation ratio (no depolarisation for liquid particles) and filtered out volcanic ash using the MIPAS volcanic ash detection algorithm (Griessbach et al., 2014). To clarify we added text on page 22, line 28, page 23, lines 1-6 in the revised manuscript (with tracked changes), accordingly.

(iii) The choice of the AIRS SO_2 index (SI) data for emission parameter estimate needs to be motivated as it might not be the most suited data set for the inversion.

The method itself is designed to be independent of the choice of meteorological data and satellite data (from the implementation point of view), although the quality of final forward simulation results may be different due to the nature of the different data sets. In this study, we used AIRS satellite observations and ERA-Interim meteorological data as input to the inversion procedure. An intercomparison of the simulation results by using our method using other meteorological and satellite data products is beyond the scope of this work.

However, note that the AIRS SO_2 index used in this study provides significant improvements compared to the NASA operational data product (Hoffmann et al., 2014). The noise level of the AIRS and IASI radiance measurements is comparable. AIRS provides observations for 2.9 million footprints per day whereas IASI provides observations only for 1.3 million footprints per day. We were also interested in exploring the capabilities of the new AIRS data product for the estimation of SO_2 emissions rather than using existing data sets.

(iv) The basic methodology needs to better be explained and case specific fine tuning should better be avoided. It requires clarification what additional information – apart

from the AIRS SI and the ERA-interim meteorological data – was fed into the inversion approach. It appears that the method does not actually provide a quantification of the emission rates. Also, the sensitivity to ad-hoc choices such threshold for plume presence in model and observations are not sufficiently discussed.

The method does not provide an estimate of the total amount of SO_2 released, but tries to optimize its relative distributions in height and time. The total mass of SO_2 for all air parcels needs to be specified as a priori information. The manuscript was revised to make this more clear (e.g., on page 17, lines 25-27, page 20, lines 1-4 in the revised manuscript with the tracked changes).

We found that fine-tuning for the Nabro case study improves the simulation results. The sensitivity study on the weight-updating schemes in Sect. 4.4 in the revised manuscript illustrates that different choices of the split point introduce some differences (cf. Figure 8 in the revised manuscript) in the estimated relative distribution of the time- and altitude-dependent SO_2 emissions. We concluded that the split point is a parameter that should be optimized for each case and added corresponding text on page 22, lines 8-11 in the revised manuscript (with tracked changes).

(v) The model does not seem to include any SO_2 loss processes (chemical conversion, deposition). The literature suggest a lifetime of about one to two a weeks. This will have an impact on emission parameter estimates.

We revised the manuscript to indicate that in the version of MPTRAC used in this study we did not consider loss processes of SO_2. Hoffmann et al. (2016) used a new version of MPTRAC, which took into account decomposition of SO_2. We found that the reconstructed emission data as well as the simulation results by means of the two different versions of MPTRAC are very similar for the time period covered by this study. In particular, the simulated distributions' patterns of SO_2 do not change, only the total mass is affected. Nevertheless, considering SO_2 loss in the future will likely provide an option for further optimization. We added text on page 27, lines 4-8 in the revised manuscript: "*Furthermore, the version of MPTRAC used in this study did not consider loss processes of SO_2. Hoffmann et al. (2016) used a newer version of MPTRAC, which takes into account loss processes of SO_2. Although the simulation results by means of the two different versions of MPTRAC are rather similar, a precise quantitative analysis considering the SO_2 loss will be subject of future efforts.*"

A positive aspect of the paper is the methodology the authors apply to evaluate the match between model and observations by using contingency tables. However, only the binary match (yes/no) w.r.t location seems to be tested. The approach should be developed further as the evaluation of volcanic plumes simulations can often not be done justice with simpler approaches.

The CSI is a frequently used measure to validate simulations of volcanic eruption events (e.g., Stunder et al., 2007; Webley et al., 2009; Harvey and Dacre, 2016). We pointed this out on page 13, lines 11-13 in the revised manuscript (with tracked changes). Nevertheless, further

statistical methods and additional quality measures can provide valuable information in future work. This aspect is also discussed by Harvey and Dacre (2016).

Specific remarks:

Abstract

Please give numbers how much the CSI improved from the constant scenario to your best estimate (max 32.3% - >41.2 and average 8.1%. ->16.6 %,)

We added this on page 2, lines 23-27 in the revised manuscript (with tracked changes).

P 9105

L 10: Using the SO_2 as proxy for ash and vice versa (as done in this paper) has to be done with caution. There are also examples of the separation of the two (Moxnes, et al. 2014 for Grimsvoetn). This point is of great importance for this paper as ash observations are used to validate the SO_2 emissions.

To clarify we added the reference and modified the text accordingly on page 3, lines 14-16 in the revised manuscript (with tracked changes): *"In practice, the presence of volcanic SO_2 can often be considered as a good proxy for the presence of volcanic ash (Sears et al., 2013), although in some cases different transport directions of SO_2 and ash were also observed because of different injection altitudes and vertical wind shear (Moxnes et al., 2014)."*

To clarify we also added text on page 22, line 28, page 23, lines 1-6: *"For the evaluation of the SO_2 heights we used MIPAS, and CALIOP H_2SO_4 (sulfate aerosol) detections. This aerosol forms from the SO_2 and hence, it can be seen as an indicator for the position of the SO_2. As other studies already found (Fromm et al., 2014; Clarisse et al., 2014) there was very little ash in the Nabro plume. However, to really make sure that we did not compare with ash, we checked the CALIOP depolarisation ratio (no depolarisation for liquid particles) and filtered out volcanic ash using the MIPAS volcanic ash detection algorithm (Griessbach et al., 2014). "*

L 17: Your collaboration in research activities is not of importance for the paper. Please omit.

We rephrased the text on page 3, lines 24-27, page 4, lines 1-2 in the revised manuscript (with tracked changes): *"In order to further improve the quality of available satellite data, e. g., to perform more effectual suppression of interfering background signals, new detection algorithms for volcanic emissions for European Space Agency (ESA) and National Aeronautics and Space Administration (NASA) satellite experiments have been developed and are used in this study (Griessbach et al., 2012, 2014; Hoffmann et al., 2014; Griessbach et al., 2015)."*

L 20: Please discuss the limitation of the satellite observations of volcanic SO_2 in more detail. Mention the consequences for the source inversions but also for the evaluation of the forward model runs.

To clarify we added the text on page 9, lines 7-13 in the revised manuscript (with tracked changes): "*The AIRS data product provides SO_2 indices for atmospheric columns, i.e., no vertical profile information on the SO_2 distributions is directly available. However, radiative transfer calculations showed (Hoffmann and Alexander, 2009; Hoffmann et al., 2016) that the SI of Hoffmann et al. (2014) is most sensitive to SO_2 layers at about 8 to 13 km altitude. Besides, nearly global coverage can only be achieved every 12 hours and there is information lacking for uncovered regions between the satellite scans. Note that the AIRS data product considered here has low noise, i.e., about 0.14 K at 250 K scene temperature*."

In general, the solution quality of an inverse problem depends on the mathematical evaluation procedure, and also on how complete and how noisy the observational data are. For example, our reconstructed time- and altitude dependent emissions match well qualitatively with those obtained by applying a simple backward trajectory approach (Hoffmann et al., 2016) for the Nabro case study. A more detailed quantitative study of the uncertainties of the inverse solutions against data uncertainties is valuable, which we would like to consider in future work. Here the focus is on introducing the method.

L 25: Please mentioned also the NAME model, which is used by the UK met-office for ash plume forecasts.

We cited the corresponding paper on page 4, lines 9-10 in the revised manuscript (with tracked changes).

P 9106

L 11: This does not make sense. Inverse techniques also use satellite data. You should have lists for the used observations and the applied techniques.

We modified the text on page 4, lines 21-26 and on page 5, lines 11-15 in the revised manuscript (with tracked changes).

L 22: Please explain "Tikhonov-type regularization" or provide reference.

Corresponding reference has been added. We modified the text on page on page 5, lines 5-6 in the revised manuscript (with tracked changes): "*A Tikhonov-type regularization method (Tikhonov and Arsenin, 1977, Seibert et al., 2000) was used to resolve the ill-posedness of the inverse problem.*".

L22: "objective function" , please clarify

In the field of mathematical optimization, an objective function, a loss function or a cost function is often defined for a minimization problem in order to find an "optimal" solution. To clarify we modified the text on page 5, lines 6-8 in the revised manuscript (with tracked changes): "*The objective function defined for the minimization problem quantifies the misfit between model values and observations, but also enforces smoothness of the solution.*"

P 9107

L 1: Why only "nadir" and not limb sounders, the latter could provide better profiles

Although we considered the nadir satellite observations for the inversion of SO_2 emission, we have to mention that our method is in general also applicable to other sort of measurements. Hence we removed the word "nadir" on page 5, line 18 to give a more general message.

L2: Please explain the main idea of "sequential importance resampling"

Sequential importance resampling is a special type of particle filter (Del Moral, 1996) that is used to estimate the posterior density of state variables given indirect observations. The method approximates the probability density by a weighted set of samples. Here we infer the probability density of "hidden" variables (i.e. the SO_2 emissions at the volcano) based on indirect observations (AIRS detections of the SO_2 plume). The method provides the relative distribution of the SO_2 emissions. To clarify we added explanation on page 11, lines 10-17 in the revised manuscript (with tracked changes).

L8: please explain the typical resolution of the discretization

For the case study of Eyjafjallajökull eruption, Stohl et al. (2011) used 19 vertical layers stacked up to 12.3 km altitude and 3-h time intervals for the discretization of the emission variable. In the work of Flemming and Inness (2013), different vertical heights between 2 and 15 km in intervals of about 2–3 km and more than 6 h time intervals were considered. In the current study, we considered a much finer discretization for the unknown time- and altitude-dependent emission variable (250 m in altitude and 1 hour in time). To clarify we added explanation on page 6, lines 11-15 in the revised manuscript (with tracked changes).

L8: please explain why this needs massive parallel computing, what is your definition of "massive"

We refer to "massive parallel" simulations because a large number of processors is used to perform a set of coordinated computations simultaneously. The volcanic emissions in the Nabro case study are strongly time- and altitude- dependent. We tried to discretize the emission domain as finely as possible. This way, we would like to reveal the local details of the emission in a relatively small temporal and spatial resolution. For each small discretized subdomain, we need to perform a unit simulation. In this specific study 15840 MPTRAC simulations for all subdomains have been performed in parallel. These calculations are repeated multiple times.

L8: please give approximate number of calculation required

During the inversion we performed 15840 unit simulations in parallel in each iteration. We added this information "(> 10000)" in the text on page 6, line 4 in the revised manuscript (with tracked changes).

L 14: Your method seems to have communalities with Flemming and Inness (2013) as they also use an ensemble of test tracers plumes and their match with observations to determine the emission parameters.

The work of Flemming and Inness (2013) used ECMWF's IFS as the forward model. In the current study, we used the Lagrangian transport model MPTRAC to perform the forward

simulations. Compared to the work of Flemming and Inness (2013), we considered a much finer discretization for the unknown time- and altitude-dependent emission source term (250 m in altitude and 1 hour in time). The Critical Success Index (CSI) was used to evaluate the goodness-of-fit of the forward simulations and to estimate the importance weights of the time- and altitude-dependent SO_2 emission. This way, we provided relative distributions of the emission in a two-dimensional view (both in time and altitude) and its local details in a relatively high temporal and spatial resolution can be revealed. To clarify we added explanation on page 6, lines 9-21 in the revised manuscript (with tracked changes).

L18: please motivate the choice of the AIRS SO_2 data. There other data sets e.g. from UV instruments such as OMI, GOME-2 or IR like IASI

Discussion and comparison of the SO_2 inversions with other satellite data have been added in the introduction and result sections. Please find more details in our response to the comments of Reviewer 1's (7. Validation).

L 20: please mention your evaluation with CALIPO and MIPAS aerosols

We added this on page 6, line 29, page 7, line 1 in the revised manuscript (with tracked changes): "*Firstly, the reconstructed altitude-resolved time series of volcanic emissions are discussed and validated with MVIRI infrared imagery and CALIOP and MIPAS aerosol measurements.*"

P 9108

L 6ff: please provide reference for mid-point method, and the approach to simulate diffusion (Markov model is a very general term). Why do you distinguish between "atmospheric diffusion" and "turbulent diffusion" ?

We added a reference on page 7, line 11 for the midpoint method. We modified the text on page 7, lines 14-15 in the revised manuscript: "*Diffusion and subgrid-scale wind fluctuations are simulated following the approach of the FLEXPART model (Stohl et al., 2005; Hoffmann et al., 2016).*".

L 8: Please explain what chemical conversion processes or removal process of SO_2 are considered. If not this may have important consequences for your results.

The version of MPTRAC used in this study does not consider the loss of SO_2. Hoffman et al. (2016) considers a new version of MPTRAC, which takes into account loss processes of SO_2. The simulations with the two versions of MPTRAC show rather similar results, especially the relative distribution of SO_2 both in time and space.

L 9-13: Why is the detail on the parallelisation of importance here? Most of the atmospheric models require high amount of parallelism. Perhaps omit.

An efficient parallelisation was considered as a main feature in the design and development of the MPTRAC model. We would prefer to keep this short statement in the paper.

P 9109

L 1: Is the 6 h time resolution of the ERA-interim data good enough for trajectory calculations. Is this a limitation of your modelling?

In a recent study of Hoffmann et al. (2016), four different meteorological products have been compared for the Nabro simulations. Simulations with MERRA (3 h resolution) showed slightly lower performance than ERA-Interim (6 h resolution). However, the MERRA data had also slightly lower spatial resolution than the ERA-Interim data. This indicates that both spatial and temporal resolution of the meteorological data sets play an important role regarding the accuracy of simulations.

L 20: What is the possible range of SI, please explain how a quantitative information can be obtained from this index.

The maximum range of SI found in the data is about 0 to 50 K, but most observations are located between 0 and 20 K. Hoffmann et al. (2014) performed radiative transfer calculations for SO_2 layers located at different heights that can be used to correlate the AIRS SO_2 index with the SO_2 column density.

P 9110

L2: How is the limitation to this height range affecting your results?

Since we assume a pre-given amount of total SO_2 emission based on the study of Clarisse et al. (2012), namely 1.5×10^9 kg, the emission rates for the equal-probability strategy will by definition vary with the chosen size of time- and altitude dependent initialization domain. In general, if the height range is chosen sufficiently large for the individual eruption case, the choice of the initialization domain will not anymore affect our results in the cases of mean rule or product rule.

Section 2.3

The evaluation of the final SO_2 forecast should use observations that represents the model result, i.e. SO_2. Therefore please evaluate with SO_2 retrieval from IASI or UV instruments such as GOME-2, OMI etc. You may use the CALIPO data or the imagery as secondary test for the injection height but you can not rely on them entirely.

We added a more detailed discussion for the validation of both emission reconstruction and forward simulation results by comparing with the work of Theys et al. (2013) and Clarisse et al. (2014). Detailed response can be found in our response to Reviewer 1's comments (7. Validation).

P 9111

L11: It is not clear how this quantification of the emission flux is achieved if only the match in location is testes with CSI

To clarify we modified the text on page 11, lines 7-17 in the revised manuscript (with tracked changes): "*In this study, an inversion approach based on the concept of sequential importance sampling (Gordon et al., 1993) in combination with different resampling*

strategies is proposed to iteratively estimate the volcanic SO_2 emission rates the relative distribution of the volcanic SO_2 emissions. Sequential importance resampling is a special type of a particle filter (Del Moral , 1996) that is used to estimate the posterior density of the state variables given the observation variables. In our case, it aims to approximate the probability density by a weighted set of N samples, namely to infer the probability densities of "'hidden"' variables (the SO_2 emissions at the volcano) based on indirect observations (AIRS detections of the SO_2 plume). The SO_2 emission rates can then be calculated indirectly by assuming that the total SO_2 mass is known a-priori.".

L25: What is the strength of the emission pulse for each of unit simulation?

In general, the number of air parcels used for the unit simulations is independent of the number of air parcels used for the final forward simulations, because only a relative distribution (relative weights) of the SO_2 emissions is the output of the inversion. For the unit simulations, we tested with numbers of air parcels ranging from a few hundreds to a few thousands, all yielded similar results for a final forward simulation with two million air parcels.

P 9112

L6: why "hidden"

In the terminology of particle filtering or sequential importance resampling the term "hidden" refers to the variables that are not directly (easily) observable. As emission rates at the volcano are usually not directly (or easily) observable, we refer to a "hidden" initialization.

Please see reply to comment on page 9107, line 2.

L12: Please make clear at what point the observations are used

To clarify we modified the text on page 12, lines 12-15 in the revised manuscript (with tracked changes): "*This way, the task of reconstructing the altitude-resolved time series of the volcanic emissions from satellite observations mathematically turns into the task of iteratively estimating the importance weight matrix W.*".

P 9113

L 9: It is not clear how you obtain the threshold of 0.1%. Is the SO_2 mass the mass of the ensemble unit simulations? What is the correspondence to the observed values. Or is it just a match between yes/no etc.

This threshold is considered as a method parameter. It defines the minimal number of air parcels that are needed to trigger a forecast event in a grid box. It needs to be adjusted to the number of air parcels used in the simulations. Based on a given total mass of all air parcels, it can also be converted into an equivalent mass per grid box or a column density. The threshold value of 0.1% used here was chosen empirically to optimize the results in the CSI analysis.

L 14: 4 DU is already a strong volcanic SO_2 signal. I could imagine that the choice of this threshold is important for the final outcome of your simulation. Please clarify.

The choice of the threshold is important as it determines the area fraction of the SO_2 plume that is validated by the CSI approach. As shown by Hoffmann et al. (2016), the threshold should be adjusted for different volcanic eruption events to cope with different sensitivity of the AIRS instrument and to obtain optimal results in the CSI analysis. For the Nabro case study we tested several values and found that 4 DU is a proper threshold value to be used.

P 9115

L 10: The choice of the split point seems important for the results. Is it just a heuristic choice. Please explain in more detail. How universal is a split point of 48 h. Please mention your sensitivity study in section 4.5

Section 3.3 provides a motivation for the product rule and for introducing the split point (cf. page 9114, line 18 – page 9115, line 13 GMDD paper). To further clarify we added text on page 22, lines 8-11 in the revised manuscript (with tracked changes): "*Note that the choice of the split point might be different for each particular volcanic eruption. A suitable value for the Nabro case study is 48 h. Nevertheless, our sensitivity analysis shows that the forward simulation results do not vary much with small changes (± 12h) of the chosen split point.*"

L 17: subdomains of the emission column?

We mean subdomains of the time- and altitude-dependent initialization domain. To clarify this we modified the text on page 16, lines 6-8 in the revised manuscript (with tracked changes): "*Furthermore, the numbers of SO_2 air parcels in all subdomains (i.e. the discretized grid boxes of the initialization domain along the time axis and the altitude axis) are scaled linearly with the corresponding importance weights.*"

P 9116

L 11: How does the number of Clarisse et al. (2012) compare with your estimate.

In this study we used the total emission estimate of 1.5×10^9 kg by Clarisse et al., (2012) as an input parameter. All schemes (equal-probability strategy, mean rule, and product rule) yield information on the relative distribution of the emission rates in the considered time- and altitude-dependent initialization domain, but do not alter the total emissions.

P 9117

L 4: the AIRS data are only available for the respective overpasses. Please specify which orbits (times) have been used for the for the emission update. How does the temporal resolution of the data impacts the results.

To clarify we modified the text on page 17, lines 18-21 in the revised manuscript (with tracked changes): "*For the reconstruction of the SO_2 emission rates we use the AIRS satellite data between 13 June 2011, 00:00 UTC and 23 June 2011 00:00 UTC, which are measured at nearly fixed local times of 01:30 and 13:30.*".

In general, from the viewpoint of inverse problems, an increase of temporal resolution of the data will improve the accuracy of the emission estimates. For example, the "jumps" the emission time series in Fig. 5 are likely due to the limited time resolution of the AIRS observations.

P 9117

L 15: Does this simulation use a constant and uniform (in the vertical) emission flux? If yes say so.

A temporal and spatial initialization domain for the volcanic emissions is selected and finely discretized for the numerical computation. The first scheme, the equal-probability strategy, assumes a constant and uniform rate in the initialization domain. To clarify this, on page 18, lines 5-6 in the revised manuscript (with tracked changes) we added: "*, which leads to constant and vertically uniform emission rates for the simulation.*"

P 9118

L 1: Please say that you only test the match in space and not the SO_2 total column value.

To clarify we modified the text on page 18, lines 15-17 in the revised manuscript (with tracked changes): "*Since the AIRS satellite data used here lack vertical information, only horizontally projected simulation results are used to test the data match in grid boxes. SO_2 column densities are not compared directly.*".

P 9119

L 3: But this all depends on the arbitrary choice of your split point.

Please see reply to comment on page 9115, line 10. The choice is considered optimal and not arbitrary. A sensitivity test is reported in Sect. 4.4 in the revised manuscript.

L 14: It is not clear where this number comes from. How did you obtain the total SO_2 burden? Please clarify.

To clarify this, on page 20, lines 1-3 in the revised manuscript (with tracked changes) we rephrased: "*By assuming a total mass of 1.5×10^9 kg for the entire initialization domain, the equal-probability strategy (first guess) considers an equal weight of wij = 1/15840 that leads to an equal emission rate of approximately 0.1052 kg m^{-1} s^{-1}.*"

L 20: Is the total emission obtained with product and mean rule the same or not. Please give numbers. The plot suggest different total emissions for the two cases.

The same total emissions of 1.5×10^9 kg are considered in this study for all schemes (equal-probability strategy, mean rule and product rule). The obtained maximum emission rates with respect to the mean rule and the product rule differ, but the integrated emissions in the considered initialization domain are the same.

P 9120

L 5: Why are they an underestimation?

We added text on page 20, lines 21-25 in the revised manuscript (with tracked changes): "*Since the total emission considered in this study (1.5×10^9 kg) is the same for all emission reconstruction schemes, and the mean rule yields some local emissions for unlikely cases (for instance at altitudes above 20 km), the emissions for more likely cases (e. g., on 13 June 2011, 00:00 UTC at 16.5 km altitude) are underestimated.*"

L 23 Figure 7 is not clear. Why is the diagram above the imagery? Perhaps two panels are better.

We put the WV images on top and IR images on bottom of the diagram by purpose. To add the reason for this, we added the following to describe Fig. 9 in more detail on page 22, lines 14-20 in the revised manuscript (with tracked changes):

"*From MVIRI WV and IR measurements (Fig. 9, top and bottom panel) we derived time series information (Fig. 9, middle panel) of the eruption history. The WV channel gives information on the high altitude eruption phase, because it gets optically thick in the middle troposphere (around 6 km) where also the AIRS SO_2 channel gets optically thick. In contrast, the IR channel reaches down to the ground and gives also information on low altitude plumes (e.g., on 17 June 2011).*"

P 9122

This whole discussions should perhaps be moved upward. In it is present from there are no real conclusions, which split point is best. Is it case specific etc.?

We moved the section of sensitivity study upward (Sect. 4.5 → Sect. 4.4).

We extended the discussion on page 22, lines 8-11 in the revised manuscript (with tracked changes): "*Note that the choice of the split point might be different for each particular volcanic eruption. A suitable value for the Nabro case study is 48 h. Nevertheless, our sensitivity analysis shows that the forward simulation results do not vary much with small perturbation (± 12 h) of the chosen split point.*"

L 25 Please discuss which one is better. Are there any recommendation for the split point choice – or not. If not it is perhaps not necessary to include this section in the paper.

The section of sensitivity analysis aims to state that a case-specific split point needs to be chosen to apply the product rule. Nevertheless, the forward simulation results actually do not vary much with small changes of the chosen split point.

P 9123

L4: "equal-probability strategy" explain that this is the uniform and constant emission scenario.

To clarify this, on page 24, lines 7-8 in the revised manuscript (with tracked changes) we added: "*Note that the equal-probability strategy assumes a constant emission rate in the entire time- and altitude-dependent initialization domain.*"

L 4: Do all emission scenarios have the same total or do they differ? Please clarify.

All three emission scenarios consider the same total mass according to Clarisse et al. (2012). On page 17, lines 25-27 in the revised manuscript (with tracked changes) we modified: *"The sum of these parcels then hold the total Nabro emission mass, which is estimated as* 1.5×10^9 *kg according to the work of Clarisse et al. (2012).*"

L 7: Are the number of "false alarms" (model = yes, obs = false) and "misses" " (model= no, obs = yes) more or less the same in the three model runs. Or does one type dominate? This would be important additional information. Please try to show also time series of these components of the CSI.

Below we compare the time series of "false alarms" and "Probability Of Detection" during 12 h time intervals obtained by applying the equal-probability strategy, the mean rule, and the product rule. The plots also confirm the message of the CSI plot, namely the use of product rule yields the best simulation results of the three cases. We added them into Fig. 10 in the revised manuscript and added corresponding text on page 14, lines 9-16, page 24, line 5, lines 17-19.

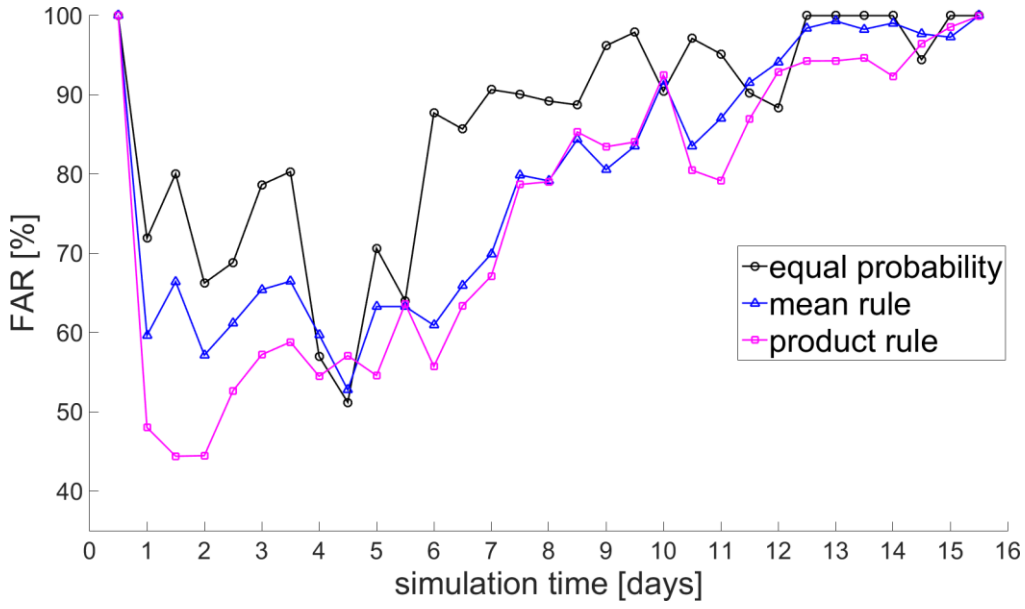

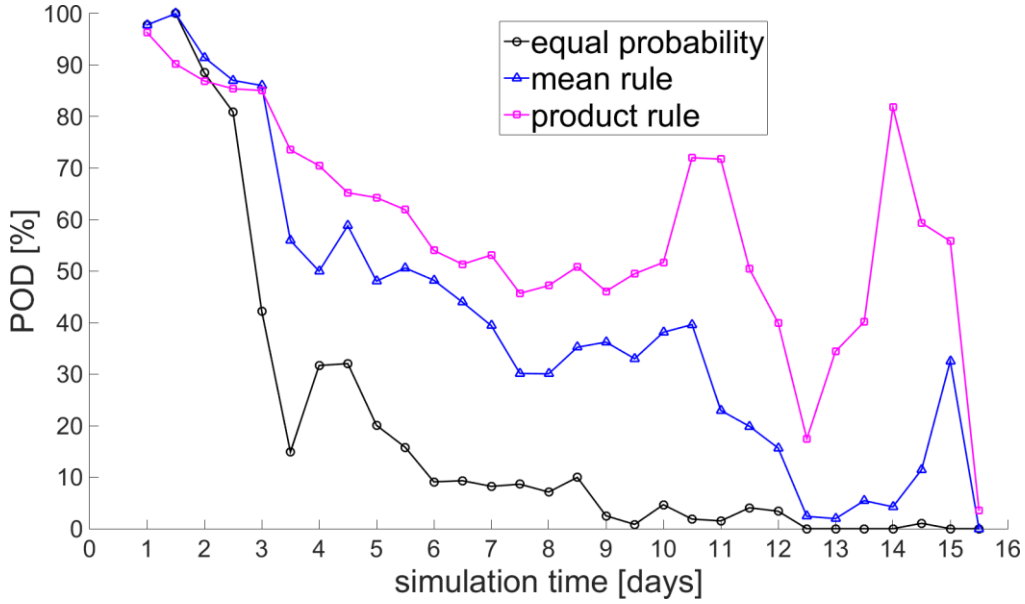

L 16: On average 16% hit is perhaps not so overwhelmingly high.

The application of the product rule provides the best simulation results of all three cases. Its maximum and mean CSI values are 52.4 and 21.4 %, respectively. The CSI values reported here are comparable to those in other studies on transport simulations for volcanic eruptions. For example, Stunder et al. (2007), Webley et al. (2009), and Harvey and Dacre (2016) mostly present CSI values between 10% and 50% for their simulations.

P 9124

L 8: Please clarify how the total emissions are assed and what the input data are and what your ad-hoc choices are.

In this study, the number of air parcels and the total mass of the SO_2 emissions are considered as inputs to the simulation system. Based on the information of the relative distribution of the SO_2 total emissions in the time- and altitude-dependent initialization domain, which is estimated by the proposed inversion algorithm, the local SO_2 emission rates can be obtained (cf. Figure 5). To clarify we added the aforementioned text on page 25, lines 22-26 in the revised manuscript (with tracked changes).

L 9: Please say more clearly what the "equal probability assumption" is.

To clarify this we added text on page 24, lines 7-8 in the revised manuscript (with tracked changes): "*Note that the equal-probability strategy assumes a constant emission rate in the entire time- and altitude-dependent initialization domain.*"

L 12: Make clear that this evaluation with the imagery is only qualitative.

We replace the word "assessed" with "qualitatively assessed" on page 26, line 3 in the revised manuscript.

L 16: Please give numbers how much the CSI improved for the three scenarios

To clarify we added text on page 26, lines 8-11 in the revised manuscript (with tracked changes): "*The mean and maximum CSI values obtained by using the equal-probability strategy are 8.1% and 32.3%, respectively. The mean rule yields a mean CSI value of 16.6% and a maximum of 41.2%. The product rule leads to an improvement of the mean CSI value to 21.4% and of the maximum CSI value to 52.4%.*"

Manuscript prepared for Geosci. Model Dev. Discuss.
with version 2015/04/24 7.83 Copernicus papers of the LaTeX class copernicus.cls.
Date: 16 February 2016

Inverse transport modeling of volcanic sulfur dioxide emissions using large-scale ~~ensemble~~ simulations

Y. Heng[1,2], L. Hoffmann[1], S. Griessbach[1], T. Rößler[1], and O. Stein[1]

[1]Forschungszentrum Jülich, Jülich Supercomputing Centre (JSC), Jülich, Germany
[2]Forschungszentrum Jülich, Institute of Energy and Climate Research – Tropospheric Research (IEK-8), Jülich, Germany

Correspondence to: Y. Heng (y.heng@fz-juelich.de)

Abstract

An inverse transport modeling approach based on the concepts of sequential importance resampling and parallel computing is presented to reconstruct altitude-resolved time series of volcanic emissions, which often can not be obtained directly with current measurement techniques. A new inverse modeling and simulation system, which implements the inversion approach with the Lagrangian transport model Massive-Parallel Trajectory Calculations (MPTRAC) is developed to provide reliable transport simulations of volcanic sulfur dioxide (SO_2). In the inverse modeling system MPTRAC is used to perform two types of simulations, i. e., ~~large-scale ensemble~~ unit simulations for the reconstruction of volcanic emissions and ~~final transport simulations~~ final forward simulations. ~~The~~Both types of transport simulations are based on wind fields of the ERA-Interim meteorological reanalysis of the European Centre for Medium Range Weather Forecasts. The reconstruction of altitude-dependent SO_2 emission time series is also based on Atmospheric Infra~~r~~Red Sounder (AIRS) satellite observations. A case study for the eruption of the Nabro volcano, Eritrea, in June 2011, with complex emission patterns, is considered for method validation. Meteosat Visible and InfraRed Imager (MVIRI) near-real-time imagery data are used to validate the temporal development of the reconstructed emissions. Furthermore, the altitude distributions of the emission time series are compared with top and bottom altitude measurements of aerosol layers obtained by the Cloud–Aerosol Lidar with Orthogonal Polarization (CALIOP) and the Michelson Interferometer for Passive Atmospheric Sounding (MIPAS) satellite instruments. The ~~final transport simulations~~ final forward simulations provide detailed spatial and temporal information on the SO_2 distributions of the Nabro eruption. ~~The SO_2 column densities from the simulations are in good qualitative agreement with the AIRS observations.~~ By using the Critical Success Index (CSI), the simulation results are evaluated with the AIRS observations. Compared to the results with an assumption of a constant flux of SO_2 emissions, our inversion approach leads to an improvement of the mean CSI value from 8.1% to 21.4% and the maximum CSI value from 32.3% to 52.4%. The simulation results are also compared with those reported in other studies and good agreement is observed. Our new

inverse modeling and simulation system is expected to become a useful tool to also study other volcanic eruption events.

1 Introduction

Observing trace gases and ash released by volcanic eruptions is important for various reasons. Most notably, sulfate aerosols formed by oxidation of SO_2 have significant impact on radiative forcing and are a natural cause for climate variations (Lamb, 1970; Robock, 2000; Solomon et al., 2011). Strong volcanic eruptions inject SO_2 directly into the lower stratosphere. However, more complex transport processes such as the Asian Monsoon circulation have also been investigated (Bourassa et al., 2012; Fromm et al., 2013; Vernier et al., 2013). Further motivation to monitor the dispersion of volcanic emissions is to prevent aircraft from entering potentially dangerous regions, i. e., flight corridors containing high loads of volcanic ash (Casadevall, 1994; Carn et al., 2009; Prata, 2009; Brenot et al., 2014). In practice, the presence of volcanic SO_2 can often be considered as a good proxy for the presence of volcanic ash (Sears et al., 2013), although in some cases different transport directions of SO_2 and ash were also observed because of different injection altitudes and vertical wind shear (Moxnes et al., 2014).

Satellite instruments are well suited to observe trace gases and aerosols on a global scale and to provide long-term records. Together, volcanic SO_2 and sulfate aerosols provide excellent tracers to study atmospheric transport processes. ~~In order to further improve the quality of available satellite data, e. g., to perform more effectual suppression of interfering background signals, we recently contributed to the development of new detection algorithms for volcanic emissions for European Space Agency (ESA) and National Aeronautics and Space Administration (NASA) satellite experiments (Griessbach et al., 2012, 2014; Hoffmann et al., 2014; Griessbach et al., 2015)~~. In order to further improve the quality of available satellite data, e. g., to perform more effectual suppression of interfering background signals, new detection algorithms for volcanic emissions for European Space Agency (ESA) and National Aeronautics and Space Administration (NASA) satellite exper-

iments have been developed and are used in this study (Griessbach et al., 2012, 2014; Hoffmann et al., 2014; Griessbach et al., 2015). However, satellite observations are often limited in temporal and spatial resolution due to their measurement principles. Therefore, atmospheric models are indispensable to study transport processes. In particular, Lagrangian particle dispersion models enable studies of transport and mixing of air masses based on the trajectories of individual air parcels. Widely used models are the Flexible Particle (FLEXPART) model (Stohl et al., 2005), the Hybrid Single-Particle Lagrangian Integrated Trajectory (HYSPLIT) model (Draxler and Hess, 1998), ~~and~~ the Lagrangian Analysis Tool (LAGRANTO) (Wernli and Davies, 1997), and the Numerical Atmospheric-dispersion Modeling Environment (NAME) (Jones et al., 2007). Recently, Massive-Parallel Trajectory Calculations (MPTRAC), a new Lagrangian transport model that is designed for large-scale ~~ensemble~~ simulations on state-of-the-art supercomputers, was developed at the Jülich Supercomputing Centre. A detailed description of MPTRAC and a comparison of the results of transport simulations for three volcanic emission events by means of different, freely available meteorological data products, can be found in Hoffmann et al. (2016).

Suitable initializations of the trajectory model, namely the altitude- and time-resolved emission data, are crucial for accurate and reliable simulations of the transport of volcanic SO_2 emissions. However, emissions usually can only be reconstructed indirectly, for instance, by empirical estimates from weather radar measurements (Lacasse et al., 2004), ~~by estimation techniques based on satellite data (Flemming and Inness, 2013; Hoffmann et al., 2015) or by inverse modeling techniques.~~ or by using satellite data (Theys et al., 2013; Clarisse et al., 2014; Hoffmann et al., 2016). ~~The work of Flemming and Inness (2013) used satellite retrievals of SO_2 total columns to estimate initial conditions for subsequent SO_2 plume forecasts by applying the Monitoring Atmospheric Composition and Climate (MACC) system (Stein et al. 2012) that is an extension of the 4D-VAR system of the European Centre for Medium Range Weather Forecasts (ECMWF). In particular, we~~ We refer to previous work (Eckhardt et al., 2008; Stohl et al., 2011; Kristiansen et al., 2012, 2015) on inverse transport modeling techniques in the context of estimating volcanic emissions. Those studies used an analytical inversion algorithm, based on Seibert (2000), for the re-

construction of volcanic ash or SO_2 emission rates. The inversion approach was applied to several case studies such as the 2010 Eyjafjallajökull and the 2014 Kelut eruptions. With respect to the mathematical setting, the estimation task was formulated as a linear inverse problem. ~~To resolve the ill-posedness of this problem, a Tikhonov-type regularization constraint was added.~~ A Tikhonov-type regularization method (Tikhonov and Arsenin, 1977; Seibert, 2000) was used to resolve the ill-posedness of the inverse problem. The objective function ~~of the problem~~ defined for the minimization problem quantifies the misfit between model values and observations, but also enforces smoothness of the solution. Several parameters such as the matrix of model sensitivities of observations to source terms and the regularization parameters that tune the smoothness of the solution needed to be provided a priori. Other work such as Flemming and Inness (2013) used satellite retrievals of SO_2 total columns to estimate initial conditions for subsequent SO_2 plume forecasts by applying the Monitoring Atmospheric Composition and Climate (MACC) system (Stein et al., 2012), which is an extension of the 4D-VAR system of the European Centre for Medium Range Weather Forecasts (ECMWF).

In this paper, we present a new inverse modeling and simulation system that can be used to establish reliable transport simulations for volcanic SO_2 emissions with available meteorological data and ~~nadir~~ satellite observations. The core of the system, an inversion approach based on the concept of sequential importance resampling (Gordon et al., 1993), is used to reconstruct altitude-dependent time series of volcanic emissions. It assumes that the volcanic SO_2 emissions distribute not only vertically above the location of the volcano (typically from 0 up to 30 km altitude), but also over a period of time (typically for a couple of days). ~~For the numerical computation, a temporal and spatial initialization domain for the volcanic emissions is selected and finely discretized. The fine temporal and spatial discretization of this domain creates a need for large-scale ensemble simulations. However, this setting is well suited for massive-parallel supercomputing architectures.~~ For the numerical computation, we discretized the emission domain as finely as technically feasible in order to reveal local details of the SO_2 emissions at high temporal and spatial resolution. This way, we expect to obtain more reliable simulation results. The fine discretization increases de-

mands on computing capabilities. Nevertheless, the resulting large computational effort can be handled by our solution approach that is well suited for massive-parallel supercomputing architectures. The time- and altitude-dependent volcanic emission rates are estimated ~~efficiently~~ iteratively by performing ~~the ensemble simulations~~ a large number (> 10000) of unit simulations in parallel with MPTRAC. ~~A distinct advantage is that the proposed inverse modeling and simulation system does not require an explicit source–receptor relationship and that its flexible design is independent of the choice of Lagrangian particle dispersion model, as long as the forward model can be applied to perform large-scale ensemble simulations.~~ A distinct advantage of this approach is that the proposed inverse modeling and simulation system requires no a-priori information on the emissions and does not require the calculation of the full source-receptor matrix. We considered a much finer discretization for the unknown time- and altitude-dependent emission function (250 m in altitude and 1 h in time in our case, about 2–3 km and more than 6 h in the case of Flemming and Inness (2013), and 19 vertical layers stacked up to 12.3 km altitude and 3 h time intervals in the case of Stohl et al. (2011)). We did not find a need to solve the ill-posed inverse problem by means of a Tikhonov or smoothing constraint. Furthermore, the Critical Success Index (CSI) was used here for the first time to evaluate the goodness-of-fit of the forward simulations and to estimate the importance weights of the time- and altitude-dependent SO_2 emission distribution. This way, we were able to provide relative distributions of the emissions in a two-dimensional view (in time and altitude) and its local details at relatively high (or even unprecedented) temporal and spatial resolution.

This paper is organized as follows: We first briefly introduce the Lagrangian transport model MPTRAC, the ERA-Interim meteorological data product, the AIRS satellite observations, and other validation data sets in Sect. 2. In Sect. 3, we present the concept of our new inverse modeling and simulation system, which ~~applies~~ uses an efficient parallel strategy ~~to perform large-scale ensemble simulations~~ for the reconstruction of volcanic emissions and to establish reliable SO_2 transport simulations. In Sect. 4, we focus on a case study of the Nabro volcano, Eritrea, whose eruption started on 12 June 2011 and lasted several days. Firstly, the reconstructed altitude-resolved time series of volcanic emissions are discussed

and validated with MVIRI infrared imagery and CALIOP and MIPAS aerosol measurements. Secondly, forward simulation results based on these initial conditions are ~~compared~~ evaluated with the AIRS satellite observations. A comparison of the simulations results with those reported in the studies of Theys et al. (2013) and Clarisse et al. (2014) is also included. Our conclusions are given in the final section.

2 Transport model and satellite data products

2.1 MPTRAC

In this study we make use of the Lagrangian transport model MPTRAC (Hoffmann et al., 2016) for the forward simulations. MPTRAC calculates the trajectories for large numbers of air parcels to represent the advection of air. The kinematic equation of motion is solved with the explicit midpoint method (Hoffmann et al., 2016). ~~Atmospheric diffusion is represented by adding random perturbations to the air parcel trajectories. The physical parameterizations for turbulent diffusion and sub-grid wind fluctuations are based on a Markov model.~~ Diffusion and subgrid-scale wind fluctuations are simulated following the approach of the FLEXPART model (Stohl et al., 2005; Hoffmann et al., 2016). A hybrid-parallelization scheme based on the Message Passing Interface (MPI) and Open Multi-Processing (OpenMP) is implemented in MPTRAC. The MPI distributed memory parallelization is applied to facilitate ensemble simulations by distributing the ensemble members on the different compute nodes of a supercomputer. Trajectory calculations of an individual ensemble member are distributed over the cores of a compute node by means of the OpenMP shared memory parallelization. This implementation enables rapid forward simulations for ensembles with large numbers of air parcels (typically on the order of 10^2 to 10^4 members per ensemble, with 10^6 to 10^8 air parcels per ensemble member). Moreover, MPTRAC provides efficient means for model output and data visualization. For further details we refer to the work of Hoffmann et al. (2016).

External meteorological data are a prerequisite for the trajectory calculations with MPTRAC. We use the latest global atmospheric reanalysis produced by ECMWF, namely the ERA-Interim data product (Dee et al., 2011). A large variety of 3 hourly surface parameters and 6 hourly upper-air parameters that cover the troposphere and stratosphere are included in the data product. Here, the ERA-Interim standard data on a $1^\circ \times 1^\circ$ longitude-latitude grid are applied. The altitude coverage ranges from the surface to 0.1 hPa with 60 model levels. The vertical resolution in the upper troposphere and lower stratosphere (UT/LS) region varies between 700 and 1200 m. The 6 hourly temporal resolution corresponds to data assimilation cycles at 00:00, 06:00, 12:00, and 18:00 UTC. A discussion of the analysis increments of the ERA-Interim data, being a figure of merit for the data quality, can be found in Dee et al. (2011). Including a case study for the Nabro eruption, Hoffmann et al. (2016) showed that ERA-Interim data provided ~~the best~~ good performance in the Lagrangian transport simulations of volcanic SO_2 with MPTRAC in comparison with three other meteorological data products.

2.2 AIRS

For inversely estimating the volcanic emissions and for validating the simulation results, we use satellite observations of volcanic SO_2 obtained by the AIRS instrument (Aumann et al., 2003; Chahine et al., 2006) aboard NASA's Aqua satellite. Aqua is in a nearly polar, sun-synchronous orbit with Equator-crossing at 01:30 a.m. and 01:30 p.m. local time. Scans in the across-track direction are carried out by means of a rotating mirror. Each scan consists of 90 footprints that correspond to 1765 km distance on the ground surface. Two adjacent scans are separated by 18 km along-track distance. While the AIRS footprint size is 13.5 km $\times$ 13.5 km at nadir, it is 41 km $\times$ 21.4 km at the scan extremes. Thermal infrared spectra (3.7 to 15.4 µm) for more than 2.9 million footprints are measured by AIRS per day.

Volcanic SO_2 can be detected efficiently from infrared radiance spectra based on brightness temperature differences (BTDs) (e. g., Karagulian et al., 2010; Clarisse et al., 2013). Here we use the BTD identified by Hoffmann et al. (2014) to detect SO_2 from AIRS 7.3 µm radiance measurements and apply their derived SO_2 index (SI) in our study. False detec-

tions related to scenes with low brightness temperatures due to deep convective clouds are filtered based on the detection scheme of Hoffmann and Alexander (2010). Hoffmann et al. (2014) demonstrated that their SI is better capable of suppressing background signals than the NASA operational SI and is well suited to trace even low SO_2 concentrations over long time periods. ~~Note that the AIRS data product that is used here provides only horizontally projected values, i. e., no vertical information on the SO_2 distributions is directly available.~~ The AIRS data product provides SO_2 indices for atmospheric columns, i.e., no vertical profile information on the SO_2 distributions is directly available. However, radiative transfer calculations showed (Hoffmann and Alexander, 2009; Hoffmann et al., 2016) that the SI of Hoffmann et al. (2014) is most sensitive to SO_2 layers at about 8 to 13 km altitude. Besides, nearly global coverage can only be achieved every 12 hours and there is information lacking for uncovered regions between the satellite scans. Note that the AIRS data product considered here has low noise, i.e., about 0.14 K at 250 K scene temperature.

2.3 Validation data sets

For validation of the temporal development of the reconstructed emissions, we consider infrared (IR, 11.5 µm) and water-vapor (WV, 6.4 µm) radiance data products from the Meteosat Visible and InfraRed Imager (MVIRI) aboard Eumetsat's Meteosat-7 (Indian Ocean Data Coverage, IODC).[1] MVIRI provides radiance images in three spectral bands from the full earth disc at 5 km × 5 km resolution (sub-satellite point) every 30 min. The MVIRI IR band overlaps with a spectral window region and is used for imaging surface and cloud top temperatures at day and night. The MVIRI WV absorption band is mainly used for determining the amount of water vapour in the upper troposphere. This band is opaque if water vapour is present, but transparent if the air is dry. The WV band can effectively be used to detect volcanic emissions in the upper troposphere because emissions from lower altitudes are blocked by water vapor absorption.

[1] Browse images from http://oiswww.eumetsat.org/IPPS/html/MTP (last access: 10 July 2015).

To verify the altitude distribution of the volcanic emissions we consider aerosol measurements from the CALIOP instrument aboard the Cloud–Aerosol Lidar and Infrared Pathfinder Satellite Observations (CALIPSO) satellite (Winker et al., 2010).[2] The spatial resolution of the CALIOP data is 1.67 km (horizontal) × 60 m (vertical) at 8 to 20 km altitude. We also consider aerosol top and bottom altitude measurements from the Michelson Interferometer for Passive Atmospheric Sounding (MIPAS) aboard the Environmental Satellite (Envisat) (Fischer et al., 2008; Griessbach et al., 2015). The spatial sampling of MIPAS in the nominal operation mode during the years 2005 to 2012 was 410 km (horizontal) × 1.5 km (vertical) at 6 to 21 km altitude (Raspollini et al., 2013). MIPAS has lower spatial resolution than CALIOP, but it is more sensitive to low aerosol concentrations due to the limb observation geometry.

We also consider the work of Theys et al. (2013) and Clarisse et al. (2014) for further validation of the reconstructed emissions as well as the forward simulation results. Satellite observations such as the second Global Ozone Monitoring Experiment (GOME-2) and the Infrared Atmospheric Sounding Interferometer (IASI) data sets were used in case studies, including the volcanic eruption of the Nabro in 2011. GOME-2, a UV/visible spectrometer covering the 240–790 nm wavelength interval with a spectral resolution of 0.2–0.5 nm (Munro et al., 2006), measures the solar radiation backscattered by the atmosphere and reflected from the surface of the Earth in a nadir viewing geometry. The instrument is in a sun-synchronous polar orbit on board the Meteorological Operational satellite-A (MetOp-A). It has an Equator crossing time of 09:30 local time on the descending node. The ground spatial resolution is about 80 km × 40 km and the full width of a GOME-2 scanning swath is 1920 km, which allows nearly daily global coverage. IASI was launched in 2006 on board MetOp-A (Clerbaux et al., 2009; Hilton et al., 2012). Global nadir measurements are obtained twice a day (at 09:30 and 21:30 mean local equatorial time). Its footprint ranges from a small to medium size, a 12 km diameter circle at nadir and an ellipse with 20 and 39 km axes at the scan extremes. Measurements of many trace gases including SO_2 are available from the IASI instrument (Clarisse et al., 2011).

[2]Browse images at http://www-calipso.larc.nasa.gov/products/lidar/browse_images/production (last access: 10 July 2015).

3 Inverse modeling and simulation system

3.1 Inversion by means of sequential importance resampling

A flow chart of the inverse modeling and simulation system proposed in this paper is shown in Fig. 1. Important system inputs consist of a specification of the time- and altitude-dependent domain for SO_2 emissions, the total number of air parcels for the final forward simulation, the satellite data, and the meteorological data. The Lagrangian transport model MPTRAC is used to perform ~~ensemble forward~~ unit simulations in a parallel manner. In this study, an inversion approach based on the concept of sequential importance sampling (Gordon et al., 1993) in combination with different resampling strategies is proposed to iteratively estimate ~~the volcanic SO_2 emission rates~~ the relative distribution of the volcanic SO_2 emissions. Sequential importance resampling is a special type of particle filter (Del Moral, 1996) that is used to estimate the posterior density of state variables given indirect observations. The method approximates the probability density by a weighted set of samples. Here we infer the probability density of "hidden" variables (i.e., the SO_2 emissions at the volcano) based on indirect observations (AIRS detections of the SO_2 plume). The method provides the relative distribution of the SO_2 emissions. The SO_2 emission rates can then be calculated by assuming that the total SO_2 mass is known a-priori. ~~The emission rates together with the final SO_2 transport simulations~~ Together with the final forward simulation results, the emission rates are the main output of the system.

We assume that the volcanic SO_2 emissions occur in a time- and altitude-dependent domain $E := [t_0, t_\mathrm{f}] \times \Omega$. Here t_0 and t_f denote the initial and final time of possible emissions, and $\Omega := [\lambda_\mathrm{c} - 0.5\Delta_\lambda, \lambda_\mathrm{c} + 0.5\Delta_\lambda] \times [\phi_\mathrm{c} - 0.5\Delta_\phi, \phi_\mathrm{c} + 0.5\Delta_\phi] \times [h_\mathrm{l}, h_\mathrm{u}]$ corresponds to a rectangular column oriented vertically and centered over the volcano. The horizontal coordinates for the volcano are defined by geographic longitude λ_c and geographic latitude ϕ_c. Note that Δ_λ and Δ_ϕ can be varied to control the area of the horizontal cross-section of the column for a particular simulation. h_l and h_u represent the lower and upper boundary of the altitude range used to constrain the emissions. We discretize the domain E along the time axis and the altitude axis with n_t and n_h uniform intervals, respectively. This leads

to $N = n_t \cdot n_h$ disjoint subdomains, for which we perform N parallel "unit simulations", correspondingly. Each unit simulation is conducted with an initialization of a given number of air parcels emitted in only one of the disjoint subdomains of E. ~~We refer to the set of all unit simulations at one iteration of the inversion procedure as an "ensemble simulation". In the iterative inversion procedure, a number of ensemble simulations are usually required to obtain suitable volcanic emission rates.~~

The N unit simulations at each iteration can be considered as a weighted set of particles, $\{(w_{ij}, s_{ij}), i = 1, \ldots, n_t, j = 1, \ldots, n_h\}$, with s_{ij} and w_{ij} representing the hidden initialization and the relative posterior probabilities of the occurrence of the air parcels for the (i, j)th-unit simulation, respectively. The importance weights w_{ij} have to satisfy the normalization condition $\sum_{i=1}^{n_t} \sum_{j=1}^{n_h} w_{ij} = 1$. By rearranging the importance weights in matrix form, we obtain $\mathbf{W} = (w_{ij})_{i=1,\ldots,n_t; j=1,\ldots,n_h}$ and use this notation in the subsequent sections. This way, the task of reconstructing the altitude-resolved time series of the volcanic emissions from satellite observations mathematically turns into the task of iteratively estimating the importance weight matrix $\mathbf{W}$. In order to find more realistic importance weights that reflect the relative distribution of emissions in the subdomains, unit simulations then have to be performed to estimate importance weights in an iterative scheme. Changes in the importance weights indicate how many air parcels should be reassigned to each subdomain and considered as new initial conditions for the next iteration. In our case, after 1-2 iterations we can already obtain rather stable importance weights that lead to good simulation results. Nevertheless, in order to establish a robust computational procedure, we defined a stopping criterion for the iterative update process (see Sect. 3.3 for details). Based on the importance weights obtained in the final iteration, the total number of SO_2 air parcels ~~for the possible emissions are~~ is redistributed in the entire initialization domain. With the reconstructed emission time series, the ~~final transport simulations~~ final forward simulations are performed.

Our inverse modeling approach is summarized in Algorithm 1. We first discretize the time- and altitude-dependent domain for SO_2 emissions and initialize air parcels in all subdomains with equal probability, i. e., distribute them in time and space uniformly (steps 1–2). Then,

as the core part of the system, an iterative procedure (steps 3–6) is used to update the importance weights by performing unit simulations and applying different weight-updating schemes (see details below). The iterative procedure ends when a given termination criterion (step 6) is satisfied. Finally, we use the calculated importance weights to resample the SO_2 air parcels in all subdomains and summarize the information in the entire initialization domain (step 7). With the reconstructed initializations, the ~~final transport simulations~~ final forward simulations are performed (step 8).

3.2 A measure of goodness-of-fit for forward simulations

To evaluate the goodness-of-fit of the forward simulations and to estimate the importance weights w_{ij}, we use the Critical Success Index (CSI) (Donaldson et al., 1975; Schaefer, 1990), adapting the approach presented by Hoffmann et al. (2016). The CSI is a frequently used measure to validate simulations of volcanic eruption events (Stunder et al., 2007; Webley et al., 2009; Harvey et al., 2016). The CSI measures the agreement between the model forecasts and the satellite observations by comparing the spatial extent of the modeled and observed SO_2 plumes over time. Model and observation data are analyzed on a $1^\circ \times 1^\circ$ longitude–latitude grid, accumulated over 12 h time periods. At mid and low latitudes there are typically two satellite overpasses per day (at 01:30 and 13:30 local time). An accumulation time interval shorter than 12 h may lead to time periods in the CSI analysis during which the satellite observations do not cover the volcanic plume at all. Therefore 12 h is a reasonable minimum time period for this analysis. A model forecast is classified as "positive" if the SO_2 amount in a grid box exceeds a certain threshold (for instance, 0.1 % of the assumed total SO_2 mass of all parcels in this case). Likewise, a satellite observation is classified as positive if the mean SI of the AIRS footprints within a grid box exceeds a given threshold. Here we use 2 K, which approximately corresponds to 4 DU (Dobson Units; $1\,\mathrm{DU} = 2.85 \times 10^{-5}\,\mathrm{kg\,m^{-2}}$) in terms of SO_2 column density (Hoffmann et al., 2014).

The CSI is calculated based on event counts of positive and negative model forecasts and satellite observations, respectively. To calculate the CSI, a 2×2 contingency table of the event counts is created first. By denoting the number of positive forecasts with positive

observations as c_x, the number of negative forecasts with positive observations as c_y, and the number of positive forecasts with negative observations as c_z, the CSI is defined as

$$\mathrm{CSI} = c_x/(c_x + c_y + c_z). \tag{1}$$

The CSI provides the ratio of successful forecasts (c_x) to the total number of forecasts that were actually made ($c_x + c_z$) or should have been (c_y). Note that the fourth element of the 2×2 contingency table, the number c_w of negative forecasts with negative observations, is not considered in the definition of the CSI. Although c_w is neglected to simply avoid cases of no interest, it should be noted that this causes the CSI to be a biased indicator of forecast skills (Schaefer, 1990). Alternative ways to evaluate the forward simulations such as the False Alarm Rate (FAR), namely the ratio of wrong predictions to the total number of forecasts,

$$\mathrm{FAR} = c_z/(c_x + c_z), \tag{2}$$

and the Probability Of Detection (POD), denoting the ratio of observations that are correctly forecasted to the total number of observations,

$$\mathrm{POD} = c_x/(c_x + c_y), \tag{3}$$

can also provide relevant information in addition to the CSI.

Since we compare simulation results with satellite observations on a discrete-time finite horizon (12 h time intervals), for each unit simulation the CSI values obtained at different times t_k can be summarized as a data vector of length n_k. We denote the data vector for the (i, j)th-unit simulation as (CSI_k^{ij}) with $k = 1, \ldots, n_k$ for later use in subsequent sections.

3.3 Iterative update of importance weights and resampling strategies

A straightforward scheme for updating the importance weights w_{ij} is given by

$$w_{ij} = m_{ij} / \sum_{a=1}^{n_t} \sum_{b=1}^{n_h} m_{ab}, \tag{4}$$

where the measure m_{ij} is defined as

$$m_{ij} = (\sum_{k=1}^{n_k} \mathrm{CSI}_k^{ij})/n_k. \quad (5)$$

Here, n_k denotes the total number of the time instants of satellite data (12 h intervals) that are used for computing the CSI values. This measure considers an equal weighting of the obtained CSI values of the time series data. As will be shown in Sect. 4, the weight-updating scheme defined by Eqs. (4) and (5), referred to as "mean rule" below, leads to simulations that can capture the basic transport dynamics for the Nabro case study pretty well. However, by definition any non-zero CSI value over the entire observation time period will result in a non-zero importance weight and hence it can not fully exclude cases in which emissions are actually not likely to occur at all. A few representative examples concerning this issue will be shown in Sect. 4.2.

In practice, new SO_2 emissions and already present SO_2 emissions from earlier times are often hard to be distinguished in an initial time period, but they are often more clearly separated at later times. Therefore, an improved measure is suggested here as

$$m_{ij} = \frac{\sum_{k=1}^{n'_k} \mathrm{CSI}_k^{ij}}{n'_k} \cdot \frac{\sum_{k=n'_k+1}^{n_k} \mathrm{CSI}_k^{ij}}{n_k - n'_k}, 1 \leq n'_k < n_k, \quad (6)$$

where n'_k is considered as a "split point" for the CSI time series. As will be demonstrated in Sect. 4, the weight-updating scheme defined by Eqs. (4) and (6), referred to as "product rule", can capture not only the basic but also the fine details of the SO_2 transport for the Nabro case study. This is achieved by putting a stronger "and" constraint on the first and second period of the CSI time series. Successful model forecasts in only one of the two time periods will not lead to high importance weights. This way, unlikely local emission patterns can be detected better and excluded, leading to more accurate simulations both globally and locally. Note that the length of the initial time period might be different for each

particular volcanic eruption. The split point is chosen at 48 h for the simulations presented here. Nevertheless, the general setting of Eq. (6) allows to control the trade-off between both time periods by tuning n'_k accordingly.

In each iteration of the inversion procedure the measures and corresponding weight-updating schemes based on the CSI data vectors of all unit simulations are evaluated. Furthermore, the numbers of SO_2 air parcels in all subdomains (i.e., the discretized grid boxes of the initialization domain along the time axis and the altitude axis) are scaled linearly with the corresponding importance weights. This resampling step redistributes the total SO_2 mass of all air parcels between the subdomains, according to the current importance weights. The iterative procedure ends when the change of importance weight matrices of successive iterations becomes sufficiently small. To quantify the change we use the relative difference d calculated as

$$d(\mathbf{W}^{l+1}, \mathbf{W}^{l}) = \frac{||\mathbf{W}^{l+1} - \mathbf{W}^{l}||_{\mathsf{F}}}{\max(||\mathbf{W}^{l+1}||_{\mathsf{F}}, ||\mathbf{W}^{l}||_{\mathsf{F}})}, l \geq 1, \tag{7}$$

where l denotes the iteration number and $||\cdot||_{\mathsf{F}}$ corresponds to the Frobenius norm,

$$||\mathbf{W}^{l}||_{\mathsf{F}} = \sqrt{\sum_{i=1}^{n_t}\sum_{j=1}^{n_h}|w_{ij}^{l}|^2}. \tag{8}$$

We selected a threshold of 1 % for the relative difference d in our simulations. In the Nabro case study the final importance weights were obtained after 3 iterations.

4 Nabro case study

4.1 Simulation setup

The Nabro is a stratovolcano located at (13°22′ N, 41°42′ E) in Eritrea, Africa. There were no historical eruptions recorded before June 2011. However, at about 20:30 UTC on 12

June 2011, a series of earthquakes resulted in a strong volcanic eruption. Volcanic activity lasted over 5 days and various plume altitudes occurred. Clarisse et al. (2012) reported a total SO_2 mass of approximately 1.5×10^9 kg in the UT/LS region based on measurements by the Infrared Atmospheric Sounding Interferometer (IASI). As a significant amount of ash was emitted, some regional flights had to be cancelled.[3] Due to the complexities of its emission patterns and transport processes related to the Asian monsoon circulation, we consider the Nabro eruption as an excellent example to validate our inverse modeling approach.

As described in Sect. 3, we here consider different types of simulations, i. e., unit simulations used for the reconstruction of the altitude-dependent time series of the Nabro SO_2 emissions and final forward simulations based on the estimated emission data. Regarding the unit simulations we assume that the SO_2 emissions occurred in the vicinity of the Nabro volcano within a horizontal area of $1^\circ \times 1^\circ$ at 0 to 30 km altitude between 12 June 2011, 12:00 UTC and 18 June 2011, 00:00 UTC. During this time period AIRS detected volcanic SO_2 in nearly 75.000 satellite footprints. Hence, the inversion of SO_2 emissions is constrained by a large number of satellite observations. For the numerical discretization of the emission domain, a time step of 1 h and an altitude step of 250 m are applied. This discretization leads to $132 \times 120 = 15\,840$ subdomains. For the reconstruction of the SO_2 emission rates we use the AIRS satellite data between 13 June 2011, 00:00 UTC and 23 June 2011 00:00 UTC, which are measured at nearly fixed local times of 01:30 and 13:30. In each iteration of the inversion procedure, 15 840 unit simulations for the subdomains were carried out. These large-scale ~~ensemble~~ simulations were performed in parallel on the Jülich Research on Petaflop Architectures (JuRoPA) supercomputer[4].

For the final forward simulations, starting on 12 June 2011, 12:00 UTC and running for 15 days, a total number of 2 million air parcels is considered. The sum of these parcels then hold the total Nabro emission mass, which is estimated as 1.5×10^9 kg according to the work of Clarisse et al. (2012). AIRS satellite data between 13 June 2011, 00:00 UTC and

[3] See http://www.bbc.com/news/world-africa-13778171 (last access: 22 June 2015).

[4] See http://www.fz-juelich.de/ias/jsc/juropa (last access: 22 June 2015).

28 June 2011, 00:00 UTC are considered to validate these simulation results. In Sect. 4.6 we compare final forward simulations obtained with different weight-updating schemes. The first scheme assumes that the SO_2 emissions have equal probability of occurrence in the initialization domain. Namely, equal importance weights, $w_{ij} = 1/15\,840$, are considered for initializations in all 15 840 subdomains, which leads to constant and vertically uniform emission rates for the simulation. This type of simulation does not require any measurement information such as the satellite observations. Although such an assumption is unrealistic in practice, it serves as a good initial condition for our inversion procedure to estimate the final importance weights with the other weight-updating schemes. By applying the mean rule and the product rule, the iterative inversion procedure reconstructs more realistic time- and altitude-dependent volcanic SO_2 emission rates than the equal-probability scheme.

4.2 Examples of unit simulations

In order to illustrate the basic idea behind the weight-updating schemes in the frame of the proposed inversion approach we first study individual unit simulations. Figures 2 to 4 show the results of the CSI analysis for three representative examples. Since the AIRS satellite data used here lack vertical information, only horizontally projected simulation results are used to test the data match in grid boxes. SO_2 column densities are not compared directly. ~~for this analysis~~. As mentioned earlier, the analysis is performed on a $1^\circ \times 1^\circ$ longitude-latitude grid.

Based on these examples, the unit simulations can be classified into three categories. In the first category, we consider the cases in which the assigned initialization in the specific subdomain yields SO_2 air parcel trajectories that ~~follow~~ match the satellite observations well. As an example, Fig. 2 shows the unit simulation with an initialization of emissions at 13 June 2011, 00:00 UTC $\pm$30 min and at (16.5 ± 0.125) km altitude. This simulation shows excellent agreement with parts of the satellite observations over the entire simulation time period. This indicates that SO_2 emissions most likely occurred in the corresponding temporal and spatial subdomain.

In the second category, we consider the cases where model forecasts quickly mismatch the satellite observations. As an example, Fig. 3 shows a model forecast related to emissions released at the same time as in the first example, but at (29 ± 0.125) km altitude. Figure 3 illustrates that the forecasts agree with the satellite observations only shortly after the volcanic eruption. After 12 h the SO_2 air parcels were already transported westwards, not agreeing with the satellite observations. Hence, this indicates that SO_2 emissions were not likely to occur in this temporal and spatial subdomain.

In the third category, successful model forecasts can be found for a longer time period compared with second category. The example presented in Fig. 4, with air parcels released at the same time but at (20 ± 0.125) km altitude, shows agreement between the model forecast and the satellite observations for about 2 days. However, the SO_2 air parcels were transported westwards and are not agreeing with the satellite observations at later times. Also in this temporal and spatial subdomain SO_2 emissions were not likely to occur.

In summary, ~~a good inverse modeling strategy should~~ our inversion approach is supposed to be able to identify and separate all cases in the aforementioned three different categories and yield suitable importance weights. As will be shown in the subsequent sections, both the mean rule and the product rule work well for the cases in the first category. They can therefore capture the basic transport dynamics. However, for less realistic situations in the second and third category the application of the mean rule still yields small importance weights. The product rule can be used to exclude these unrealistic cases and yield proper importance weights by choosing a suitable split point of the obtained CSI time series. As will be shown in Sect. 4.6, it is therefore considered as a superior strategy, both qualitatively and quantitatively.

4.3 Reconstruction of volcanic SO_2 emissions

Suitable initializations are necessary in order to perform reliable final forward simulations. For this purpose we estimate the time- and altitude-dependent volcanic SO_2 emissions with the iterative inversion approach outlined in Sect. 3. The time- and altitude-resolved emission rates are estimated based on the different weight-updating schemes. ~~The simple~~

~~equal-probability strategy (first guess) assumes~~ By assuming a total mass of 1.5×10^9 kg for the entire initialization domain, the equal-probability resampling strategy (first guess) considers an equal weight of $w_{ij} = 1/15\,840$ that leads to ~~an equal~~ constant and vertically uniform emission rates of approximately $0.1052\,\mathrm{kg\,m^{-1}\,s^{-1}}$ ~~in the entire initialization domain~~. However, note that such an assumption is in general not very realistic, even by posing further time- and altitude-constraints, because volcanic eruptions often change over time significantly and emissions are also not uniformly distributed with altitude.

Figure 5 shows the temporally and spatially resolved SO_2 emission rates reconstructed by applying the mean rule and the product rule, respectively. The application of the mean rule results in temporally and spatially broader areas with smaller emission rates (Fig. 5, top) up to about $1.5\,\mathrm{kg\,m^{-1}\,s^{-1}}$. As shown in the figure, some unlikely cases of local emissions mentioned in Sect. 4.2~~, e. g., at altitudes above 20 km or below 5 km,~~ are not excluded. ~~Since the total amount of emitted SO_2 is fixed, the emission rates of likely local emissions (e. g., on 13 June 2011, 00:00 UTC at altitude 16.5 km) are underestimated.~~ In contrast, the application of the product rule emphasizes the more likely cases and excludes unlikely cases (Fig. 5, bottom). Its maximum emission rate is about 6 times larger than that of the mean rule. In particular, the peak emission rates on 13 June 2011, 00:00 UTC, 14 June 2011, 15:00 UTC, and 16 June 2011, 10:00 UTC are approximately $9.28\,\mathrm{kg\,m^{-1}\,s^{-1}}$, $0.57\,\mathrm{kg\,m^{-1}\,s^{-1}}$, and $0.70\,\mathrm{kg\,m^{-1}\,s^{-1}}$, respectively. The corresponding peak emission rates estimated by the mean rule are approximately $1.50\,\mathrm{kg\,m^{-1}\,s^{-1}}$, $0.56\,\mathrm{kg\,m^{-1}\,s^{-1}}$, and $0.42\,\mathrm{kg\,m^{-1}\,s^{-1}}$~~, which are likely to be underestimated~~. Since the total emission considered in this study (1.5×10^9 kg) is the same for all emission reconstruction schemes, and the mean rule yields some local emissions for unlikely cases (for instance at altitudes above 20 km), the emissions for more likely cases (e. g., on 13 June 2011, 00:00 UTC at 16.5 km altitude) are underestimated.

Our results qualitatively agree with the emission data reconstructed by the backward-trajectory approach presented by ~~Hoffmann et al. (2016, Figs. 6 and 14)~~ (Hoffmann et al., 2016). The maximum emission rates obtained by the backward-trajectory approach are in between the maximum values obtained with the mean rule and the product rule weight-

updating schemes used here. Even closer agreement with the backward-trajectory approach might be achieved by tuning the split point of the product rule accordingly. A sensitivity study for this important tuning parameter will be presented in Sect. 4.4.

Finally, Fig. 6 shows the reconstructed emission rates integrated over time and altitude, respectively. As found earlier, the maximum emission rates for the main eruption on 13 June obtained by the product rule are much higher (up to a factor of 2 for the integrated values) than those obtained by the mean rule. However, this is compensated by lower emission rates by the product rule from 14 to 17 June. Considering the altitude distribution, Fig. 6 (bottom) reveals, especially for the product rule, that most SO_2 emissions occurred at 10 to 12 and 15 to 17 km altitude. We find that the altitude distribution is less constrained for the mean rule than for the product rule.

4.4 Sensitivity analysis for the weight-updating schemes

In this section, we first discuss the effect of different choices of the parameter n_k for the mean rule weight-updating scheme. As discussed in Sect. 3.2, n_k denotes the total number of discrete-time intervals used for the CSI analysis. It directly corresponds to the choice of the final time step of the satellite data. For the reference simulations we have chosen 23 June 2011, 00:00 UTC as the final time, corresponding to $n_k = 21$. Figure 7 (top) displays a contour plot of the importance weights for the reference case. Figure 7 (middle and bottom) shows the absolute differences with respect to other final times. By choosing 22 June 2011, 00:00 UTC ($n_k = 19$) and 24 June 2011, 00:00 UTC ($n_k = 23$) as the final times, the relative differences of the importance weights are about 9.5 and 10 %, respectively. The choice of 22 June 2011, 12:00 UTC ($n_k = 20$) and 23 June 2011, 12:00 UTC ($n_k = 22$) as final time lead to smaller relative differences, about 7.2 and 6.2 %, respectively (not shown). Based on a visual inspection, the aforementioned different importance weights all show rather similar results in the final forward simulations.

For the product rule, we performed a sensitivity analysis with n_k corresponding to the reference date (23 June 2011, 00:00 UTC), but we choose five different split points n'_k, corresponding to 24 h, 36 h, 48 h, 60 h, and 72 h after the beginning of the simulation (13

June 2011, 00:00 UTC). Considering 48 h as the reference case, the choice of the other split points lead to 23.1, 11.3, 8.7, and 13.7 % relative differences of the importance weights. Except in the case of 24 h, which is too short to constrain the time and altitude distribution of the SO_2 emissions properly, the other three cases lead to weights close to the reference and similar results in the final forward simulations. Figure 8 illustrates the results of this sensitivity test. It shows the importance weights for the reference split point (48 h) and the absolute differences of the importance weights for split points at 36 and 60 h, respectively. Note that the choice of the split point might be different for each particular volcanic eruption. A suitable value for the Nabro case study is 48 h. Nevertheless, our sensitivity analysis shows that the forward simulation results do not vary much with small perturbation (± 12 h) of the chosen split point.

4.5 Validation of emission time series

~~In Fig. 7 we show time series information for the Nabro eruption that are obtained from MVIRI IR and WV measurements aboard Meteosat-7 (IODC).~~ From MVIRI WV and IR measurements aboard Meteosat-7 (IODC) (Fig. 9, top and bottom panel) we derived time series information (Fig. 9, middle panel) of the eruption history. The WV channel gives information on the high altitude eruption phase, because it gets optically thick in the middle troposphere (around 6 km) where also the AIRS SO_2 channel gets optically thick. In contrast, the IR channel reaches down to the ground and gives also information on low altitude plumes (e.g., on 17 June 2011). The satellite imagery indicates that the strongest eruptions occurred between 13 June 2011, 00:00 and 12:00 UTC. A series of smaller emission events until 16 June 2011, 15:00 UTC were also observed. In particular, there were two short-time periods of strong eruptions on 14 and and 16 June 2011, respectively. The emission time series derived with our inverse modeling approach are in good temporal agreement with the MVIRI observations.

Injection altitudes of the Nabro eruption have been discussed recently, mostly based on different satellite measurements (Bourassa et al., 2012; Fromm et al., 2013; Vernier et al., 2013; Fromm et al., 2014). For the evaluation of the SO_2 heights we used MIPAS and

CALIOP H_2SO_4 (sulfate aerosol) detections. This aerosol forms from the SO_2 and hence, it can be seen as an indicator for the position of the SO_2. As other studies already found (Fromm et al., 2014; Clarisse et al., 2014) there was very little ash in the Nabro plume. However, to really make sure that we did not compare with ash, we checked the CALIOP depolarisation ratio (no depolarisation for liquid particles) and filtered out volcanic ash using the MIPAS volcanic ash detection algorithm (Griessbach et al., 2014). The first CALIOP measurements found the initial plume at 11–15.5 km over Pakistan and at 15–16.5 km over Iran on 15 June. Plumes were measured at 18–19 km and 8.5 –11.5 km over Egypt, at 16–17.5 km over Turkey, at 8.5–11 km over the Arabian Peninsula, at 16–17 km over Iran, and at 14–16.2 km over China on 16 June. MIPAS detected the aerosol resulting from Nabro eruption at 12–16.5 km over Israel on 14 June. The aerosol layers nearest to the Nabro were measured at 11–16.5 km on 15 June. They reached 16–18.5 km on 16 June and 12–15.5 km on 17 June. The altitudes measured by CALIOP and MIPAS agree within their uncertainties.

The relatively inhomogeneous plume altitudes can also be seen in our reconstructed emission time series, indicating multiple segregated eruption events. The first eruption on 13 June was the strongest and mainly reached altitudes of 15–17 km. This is confirmed by CALIOP and MIPAS measurements that even found aerosol up to 19 km (in low concentrations). Clarisse et al. (2014) also reported that the early Nabro plume mostly raised to altitudes between 15 and 17 km, which agrees well with our reconstructed emission time series (cf. Fig. 5). On 14 June the second eruption injected the volcanic emissions into altitudes of 9–13 km. At these altitudes aerosols were also measured by CALIOP and MIPAS. Starting from the afternoon of 15 June to 16 June, the injection altitude increased again to about 17 km, although emission rates are lower than for the first and second eruption. This is confirmed by MIPAS measurements over Egypt on 17 June reaching up to 17.5 km. Fromm et al. (2013) and Vernier et al. (2013) reported that the initial eruption on 13 June reached altitudes between 15 and 19 km, which is in good agreement with our reconstructed plume. Fromm et al. (2014) reported an injection altitude of 17.4 km for the third eruption on 16 June, which is less than 1 km above our reconstructed injection altitude. This initial

validation with the different satellite observations indicates that our reconstructed emission time series are reliable.

4.6 Final forward simulations

We performed the final forward simulations for the Nabro case study with the initializations obtained in Sect. 4.3. Figure 10 shows the corresponding CSI, POD, and FAR time series based on 12 h time intervals, obtained by applying the equal-probability strategy, the mean rule, and the product rule, respectively. Note that the equal-probability strategy assumes a constant emission rate in the entire time- and altitude-dependent initialization domain. In all cases, the largest CSI values are found at the beginning of the simulations, followed by an overall decrease towards the end of the simulation. The equal-probability strategy yields a maximum CSI value of 32.3 % and a mean CSI value of 8.1 %. The inversions that apply the mean rule and the product rule both lead to higher CSI values. The mean rule yields better simulation results than the equal-probability strategy, because it takes into account the temporal variations and inhomogeneous plume altitudes of the volcanic eruption. Its maximum and mean CSI values are 41.2 and 16.6 %, respectively. The application of the product rule provides the best simulation results of all three cases. Its maximum and mean CSI values are 52.4 and 21.4 %, respectively. Our findings for the CSI are confirmed by the FAR and POD time series (Fig. 10, lower panels), which indicates that the use of product rule yields the best simulation results of the three cases.

Figures 11 to 17 compare the simulation results with AIRS satellite observations for selected time steps. SO_2 column densities from the model are presented on a $0.5° \times 0.5°$ longitude-latitude grid. The AIRS SO_2 index during corresponding 12 h time periods is presented on the measurement grid of the instrument. In the case of the equal-probability strategy, unrealistic transport of air parcels westward of the Nabro is found. Accordingly, the estimated SO_2 column densities for realistic pathways are significantly lower. In the case of the mean rule, more realistic forecasts of the basic SO_2 transport patterns are obtained. The simulation results are qualitatively closer to the satellite observations both in time and space. However, unrealistic westward transport of SO_2 is still recognizable. The product rule

clearly yields the most reliable simulation results of the three cases. It most successfully excludes unlikely local emission patterns.

Our simulation by means of the product rule and AIRS satellite observations yields similar relative horizontal distributions of SO_2 on 15 June 2011 compared with IASI satellite data and FLEXPART model output as reported by Theys et al. (2013, Fig. 10a). Simulation results for other days, e.g., for 16, 18 and 20 June 2011 are also similar to the GOME-2 satellite retrievals reported by Theys et al. (2013, Fig. 10b – Fig. 10d). Our simulations (Fig. 12 and Fig. 14) show more realistic transport patterns on 14 and 16 June 2011 than the FLEXPART model outputs based on the IASI data (Theys et al., 2013, Fig. 12). Besides, the SO_2 distributions on 16 June 2011 and 18 June 2011 in China are not well captured by the FLEXPART model outputs based on the GOME-2 data (Theys et al., 2013, Fig. 10b and Fig. 10c), but by our simulations (Fig. 14 and Fig. 15). Furthermore, the SO_2 transport patterns of our simulations are in good agreement with IASI observations that were extensively studied in the context of the Nabro eruption (Clarisse et al., 2014, Figs. 6–10).

5 Conclusions and outlook

In this paper, we presented an inversion approach based on the concept of sequential importance resampling for the reconstruction of volcanic emission rates from infrared nadir satellite observations. Based on the proposed inversion approach, a new inverse modeling and simulation system, implemented with the Lagrangian transport model MPTRAC, has been developed to enable efficient and reliable transport simulations of volcanic SO_2 emissions. Our solution is in general independent of the choice of forward transport model and well suited for massive-parallel supercomputing architectures. The number of air parcels and the total mass of SO_2 emission are considered as inputs to the simulation system. Based on the information of the relative distribution of the SO_2 total emissions in the time- and altitude-dependent initialization domain, which is estimated by the proposed inversion algorithm, the local SO_2 emission rates can be obtained.

Together with the equal-probability assumption, two weight-updating schemes, referred to as the mean rule and product rule have been proposed for the reconstruction of emission data. Considering the Nabro eruption in June 2011 as a case study, we qualitatively assessed the reconstructed emission time series by comparing them with Meteosat-7 (IODC) imagery to validate the temporal development and with CALIOP and MIPAS satellite observations to confirm the injection altitudes. Simulation results based on the initializations reconstructed by different weight-updating schemes have been compared, in particular, to demonstrate the advantages of the product rule. The mean and maximum CSI values obtained by using the equal-probability strategy are 8.1% and 32.3%, respectively. The mean rule yields a mean CSI value of 16.6% and a maximum of 41.2%. The product rule leads to an improvement of the mean CSI value to 21.4% and of the maximum CSI value to 52.4%. The simulation results for the Nabro case study show good agreement with the AIRS satellite observations in terms of SO_2 horizontal distributions and have been validated through other independent data sets such as IASI and GOME-2 satellite observations reported by other studies. The simulation results show that the inverse modeling system successfully identified the complex volcanic emission pattern of the Nabro eruption, and helped to further reveal the complex transport processes through the Asian monsoon circulation.

Some topics were explicitly excluded from this paper, but may be investigated in future work, including the extension of the current approach towards near-real-time forecasting ~~and~~, the development of an adaptive strategy for discretizing the initialization domain, the consideration of the SO_2 kernel functions, and a detailed treatment of data uncertainties. An adaptive strategy is expected to reduce the computational effort and to provide better resolution in areas of the initialization domain where there is large variability. This way, we would expect more precise importance weights estimated for the most likely cases of local emission and hence more accurate simulation results with better local details in a quantitative manner. In particular, the SO_2 kernel functions of the AIRS channels used to calculate the SI depend on atmospheric conditions and altitude (e.g., Hoffmann et al. (2016, Fig. 1)). However, variations in the UT/LS region where most of the Nabro emissions occurred are not too large. Hence, we did not consider this dependency in our analysis. However, the

consideration of the AIRS kernel functions in the CSI analysis will be an important aspect in future work. Uncertainties in the meteorological data are another important source of error. The topic is addressed in a recent study by Hoffmann et al. (2016), wherein four different meteorological products have been tested for the MPTRAC simulations. This work aims to introduce an inversion approach for SO_2 transport simulations. A more detailed, quantitative study of the errors resulting from the uncertainties of different meteorological data will be considered in future work. Furthermore, the version of MPTRAC used in this study did not consider loss processes of SO_2. Hoffmann et al. (2016) used a newer version of MPTRAC, which takes into account loss processes of SO_2. Although the simulation results by means of the two different versions of MPTRAC are rather similar, a precise quantitative analysis considering the SO_2 loss will be subject of future efforts. Further research shall also be devoted to the testing of the proposed MPTRAC-based inverse modeling and simulation system for other case studies of volcanic eruptions and its capacity for forecasting.

Code and data availability

The current release of the MPTRAC model can be downloaded from the model web site at http://www.fz-juelich.de/ias/jsc/mptrac. The code version used in this study can be obtained by contacting the corresponding author. The time- and altitude-dependent emission time series obtained with the different weight-updating schemes (Fig. 5) are provided as an electronic supplement to this paper. This allows our results to be reproduced and extended in further work, for instance by performing simulations with other transport models.

The Supplement related to this article is available online at doi:10.5194/gmdd-0-1-2016-supplement.

Acknowledgements. AIRS data products were obtained from the NASA Goddard Earth Sciences Data Information and Services Center (GES DISC). ERA-Interim data were obtained from the European Centre for Medium-Range Weather Forecasts (ECMWF). The authors gratefully acknowledge

the computing time granted on the supercomputer JuRoPA at the Jülich Supercomputing Centre (JSC).

The article processing charges for this open-access publication were covered by a Research Centre of the Helmholtz Association.

References

Aumann, H. H., Chahine, M. T., Gautier, C., Goldberg, M. D., Kalnay, E., McMillin, L. M., Revercomb, H., Rosenkranz, P. W., Smith, W. L., Staelin, D. H., Strow, L. L., and Susskind, J.: AIRS/AMSU/HSB on the Aqua Mission: design, science objective, data products, and processing systems, IEEE T. Geosci. Remote, 41, 253–264, 2003.

Bourassa, A. E., Robock, A., Randel, W. J., Deshler, T., Rieger, L. A., Lloyd, N. D., Llewellyn, E. J. T., and Degenstein, D. A.: Large volcanic aerosol load in the stratosphere linked to Asian Monsoon transport, Science, 337, 78–81, 2012.

Brenot, H., Theys, N., Clarisse, L., van Geffen, J., van Gent, J., Van Roozendael, M., van der A, R., Hurtmans, D., Coheur, P.-F., Clerbaux, C., Valks, P., Hedelt, P., Prata, F., Rasson, O., Sievers, K., and Zehner, C.: Support to Aviation Control Service (SACS): an online service for near-real-time satellite monitoring of volcanic plumes, Nat. Hazards Earth Syst. Sci., 14, 1099–1123, doi:10.5194/nhess-14-1099-2014, 2014.

Carn, S. A., Krueger, A. J., Krotkov, N. A., Yang, K., and Evans, K.: Tracking volcanic sulfur dioxide clouds for aviation hazard mitigation, Nat. Hazards, 51, 325–343, 2009.

Casadevall, T. J.: The 1989-1990 eruption of Redoubt Volcano, Alaska: impacts on aircraft operations, J. Volcanol. Geoth. Res., 62, 301–316, 1994.

Chahine, M. T., Pagano, T. S., Aumann, H. H., Atlas, R., Barnet, C., Blaisdell, J., Chen, L., Divakarla, M., Fetzer, E. J., Goldberg, M., Gautier, C., Granger, S., Hannon, S., Irion, F. W., Kakar, R., Kalnay, E., Lambrigtsen, B. H., Lee, S., Marshall, J. L., McMillan, W. W., McMillin, L., Olsen, E. T., Revercomb, H., Rosenkranz, P., Smith, W. L., Staelin, D., Strow, L. L., Susskind, J., Tobin, D., Wolf, W., and Zhou, L.: AIRS: improving weather forecasting and providing new data on greenhouse gases, B. Am. Meteorol. Soc., 87, 911–926, 2006.

Clarisse, L., R'Honi, Y., Coheur, P.-F., Hurtmans, D., and Clerbaux, C.: Thermal infrared nadir observations of 24 atmospheric gases, Geophys. Res. Lett., 38, L10802, doi:10.1029/2011GL047271,2011.

Clarisse, L., Hurtmans, D., Clerbaux, C., Hadji-Lazaro, J., Ngadi, Y., and Coheur, P.-F.: Retrieval of sulphur dioxide from the infrared atmospheric sounding interferometer (IASI), Atmos. Meas. Tech., 5, 581–594, doi:10.5194/amt-5-581-2012, 2012.

Clarisse, L., Coheur, P.-F., Prata, F., Hadji-Lazaro, J., Hurtmans, D., and Clerbaux, C.: A unified approach to infrared aerosol remote sensing and type specification, Atmos. Chem. Phys., 13, 2195–2221, doi:10.5194/acp-13-2195-2013, 2013.

Clarisse, L., Coheur, P.-F., Theys, N., Hurtmans, D., and Clerbaux, C.: The 2011 Nabro eruption, a SO_2 plume height analysis using IASI measurements, Atmos. Chem. Phys., 14, 3095—3111, doi:10.5194/acp-14-3095-2014,2014.

Clerbaux, C., Boynard, A., Clarisse, L., George, M., Hadji-Lazaro, J., Herbin, H., Hurtmans, D., Pommier, M., Razavi, A., Turquety, S., Wespes, C., and Coheur, P.-F.: Monitoring of atmospheric composition using the thermal infrared IASI/MetOp sounder, Atmos. Chem. Phys., 9, 6041–6054, doi:10.5194/acp-9-6041-2009,2009.

Dee, D. P., Uppala, S. M., Simmons, A. J., Berrisford, P., Poli, P., Kobayashi, S., Andrae, U., Balmaseda, M. A., Balsamo, G., Bauer, P., Bechtold, P., Beljaars, A. C. M., van de Berg, L., Bidlot, J., Bormann, N., Delsol, C., Dragani, R., Fuentes, M., Geer, A. J., Haimberger, L., Healy, S. B., Hersbach, H., Hólm, E. V., Isaksen, L., Kållberg, P., Köhler, M., Matricardi, M., McNally, A. P., Monge-Sanz, B. M., Morcrette, J.-J., Park, B.-K., Peubey, C., de Rosnay, P., Tavolato, C., Thépaut, J.-N., and Vitart, F.: The ERA-Interim reanalysis: configuration and performance of the data assimilation system, Q. J. Roy. Meteor. Soc., 137, 553–597, 2011.

Del Moral, P.: Non Linear Filtering: Interacting Particle Solution, Markov Processes and Related Fields, 2 (4), 555–580, 1996.

Donaldson, R., Dyer, R. M., and Kraus, M. J.: Objective evaluator of techniques for predicting severe weather events, B. Am. Meteor. Soc., 56, 755–755, 1975.

Draxler, R. R. and Hess, G. D.: An overview of the HYSPLIT_4 modeling system of trajectories, dispersion, and deposition, Aust. Meteorol. Mag., 47, 295–308, 1998.

Eckhardt, S., Prata, A. J., Seibert, P., Stebel, K., and Stohl, A.: Estimation of the vertical profile of sulfur dioxide injection into the atmosphere by a volcanic eruption using satellite column measurements and inverse transport modeling, Atmos. Chem. Phys., 8, 3881–3897, doi:10.5194/acp-8-3881-2008, 2008.

Fischer, H., Birk, M., Blom, C., Carli, B., Carlotti, M., von Clarmann, T., Delbouille, L., Dudhia, A., Ehhalt, D., Endemann, M., Flaud, J. M., Gessner, R., Kleinert, A., Koopman, R., Langen, J., López-Puertas, M., Mosner, P., Nett, H., Oelhaf, H., Perron, G., Remedios, J., Ridolfi, M., Stiller, G., and Zander, R.: MIPAS: an instrument for atmospheric and climate research, Atmos. Chem. Phys., 8, 2151–2188, doi:10.5194/acp-8-2151-2008, 2008.

Flemming, J. and Inness, A.: Volcanic sulfur dioxide plume forecasts based on UV satellite retrievals for the 2011 Grímsvötn and the 2010 Eyjafjallajökull eruption, J. Geophys. Res., 118, 10–172, 2013.

Fromm, M., Nedoluha, G., and Charvát, Z.: Comment on "Large Volcanic Aerosol Load in the Stratosphere Linked to Asian Monsoon Transport", Science, 339, 647-c, doi:10.1126/science.1228605, 2013.

Fromm, M., Kablick III, G., Nedoluha, G., Carboni, E., Grainger, R., Campbell, J., and Lewis, J.: Correcting the record of volcanic stratospheric aerosol impact: Nabro and Sarychev Peak, J. Geophys. Res., 119, 10343–10364, 2014.

Gordon, N. J., Salmond, D. J., and Smith, A. F. M.: Novel approach to nonlinear/non-Gaussian Bayesian state estimation, Radar and Signal Processing, IEE Proceedings F, 140, 107–113, 1993.

Griessbach, S., Hoffmann, L., von Hobe, M., Müller, R., Spang, R., and Riese, M.: A six-year record of volcanic ash detection with Envisat MIPAS, in: Proceedings of ESA ATMOS 2012, European Space Agency, ESA Special Publication SP-708 (CD-ROM), 2012.

Griessbach, S., Hoffmann, L., Spang, R., and Riese, M.: Volcanic ash detection with infrared limb sounding: MIPAS observations and radiative transfer simulations, Atmos. Meas. Tech., 7, 1487–1507, doi:10.5194/amt-7-1487-2014, 2014.

Griessbach, S., Hoffmann, L., Spang, R., von Hobe, M., Müller, R., and Riese, M.: Infrared limb emission measurements of aerosol in the troposphere and stratosphere, Atmos. Meas. Tech. Discuss., 8, 4379–4412, doi:10.5194/amtd-8-4379-2015, 2015.

Harvey, N. J., and Dacre, H. F.: Spatial evaluation of volcanic ash forecasts using satellite observations, Atmos. Chem. Phys., 16, 861–872, doi:10.5194/acp-16-861-2016 2016.

Hilton, F., Armante, R., August, T., Barnet, C., Bouchard, A., Camy-Peyret, C., Capelle, V., Clarisse, L., Clerbaux, C., Coheur, P.-F., Collard, A., Crevoisier, C., Dufour, G., Edwards, D., Faijan, F., Fourrié, N., Gambacorta, A., Goldberg, M., Guidard, V., Hurtmans, D., Illingworth, S., Jacquinet-Husson, N., Kerzenmacher, T., Klaes, D., Lavanant, L., Masiello, G., Matricardi, M., McNally, A., Newman, S., Pavelin, E., Payan, S., Péquignot, E., Peyridieu, S., Phulpin, T., Remedios, J., Schlüssel, P., Serio, C., Strow, L., Stubenrauch, C., Taylor, J., Tobin, D., Wolf, W., and

Zhou, D.: Hyperspectral Earth Observation from IASI: Five Years of Accomplishments, Bull. Amer. Meteor. Soc., 93, 347—370, 2012.

Hoffmann, L. and Alexander, M. J.: Retrieval of stratospheric temperatures from Atmospheric Infrared Sounder radiance measurements for gravity wave studies, J. Geophys. Res., 114, D07105, doi:10.1029/2008JD011241, 2009.

Hoffmann, L. and Alexander, M. J.: Occurrence frequency of convective gravity waves during the North American thunderstorm season, J. Geophys. Res., 115, D20111, doi:10.1029/2010JD014401, 2010.

Hoffmann, L., Griessbach, S., and Meyer, C. I.: Volcanic emissions from AIRS observations: detection methods, case study, and statistical analysis, Proc. SPIE, 9242, 924214–924214-8, doi:10.1117/12.2066326, 2014.

Hoffmann, L., Rößler, T., Griessbach, S., Heng, Y., and Stein, O.: Lagrangian transport simulations of volcanic sulfur dioxide emissions: impact of meteorological data products, J. Geophys. Res., submitted, 2015.

Jones, A., Thomson, D., Hort, M., and Devenish, B.: Volcanic emissions from AIRS observations: The UK Met Office's next-generation atmospheric dispersion model, NAME III, in Air Pollution Modeling and its Application XVII, pp. 580-589, Springer, 2007.

Karagulian, F., Clarisse, L., Clerbaux, C., Prata, A. J., Hurtmans, D., and Coheur, P. F.: Detection of volcanic SO_2, ash, and H_2SO_4 using the Infrared Atmospheric Sounding Interferometer (IASI), J. Geophys. Res., 115, D00L02, doi:10.1029/2009JD012786, 2010.

Kristiansen, N. I., Stohl, A., Prata, A. J., Bukowiecki, N., Dacre, H., Eckhardt, S., Henne, S., Hort, M. C., Johnson, B. T., Marenco, F., Neininger, B., Reitebuch, O., Seibert, P., Thomson, D. J., Webster, H. N., and Weinzierl, B.: Performance assessment of a volcanic ash transport model mini-ensemble used for inverse modeling of the 2010 Eyjafjallajökull eruption, J. Geophys. Res., 117, D00U11, doi:10.1029/2011JD016844, 2012.

Kristiansen, N. I., Prata, A. J., Stohl, A., and Carn, S. A.: Stratospheric volcanic ash emissions from the 13 February 2014 Kelut eruption, Geophys. Res. Lett., 42, 588–596, 2015.

Lacasse, C., Karlsdóttir, S., Larsen, G., Soosalu, H., Rose, W., and Ernst, G.: Weather radar observations of the Hekla 2000 eruption cloud, Iceland, B. Volcanol., 66, 457–473, 2004.

Lamb, H. H.: Volcanic dust in the atmosphere, with a chronology and assessment of its meteorological significance, Philos. T. Roy. Soc. A, 266, 425–533, 1970.

Moxnes, E. D., Kristiansen, N. I., Stohl, A., Clarisse, L., Durant, A., Weber, K., and Vogel, A.: Separation of ash and sulfur dioxide during the 2011 Grímsvötn eruption, J. Geophys. Res., 119, 7477–7501, doi:10.1002/2013JD021129, 2014.

Munro, R., Eisinger, M., Anderson, C., Callies, J., Corpaccioli, E., Lang, R., Lefebvre, A., Livschitz, Y., and Albinana, A. P.: GOME-2 on MetOp, in: Proceedings of The 2006 EUMETSAT Meteorological Satellite Conference, Helsinki, Finland, 12–16 June 2006, EUMETSAT p. 48, 2006.

Prata, A. J.: Satellite detection of hazardous volcanic clouds and the risk to global air traffic, Nat. Hazards, 51, 303–324, 2009.

Raspollini, P., Carli, B., Carlotti, M., Ceccherini, S., Dehn, A., Dinelli, B. M., Dudhia, A., Flaud, J.-M., López-Puertas, M., Niro, F., Remedios, J. J., Ridolfi, M., Sembhi, H., Sgheri, L., and von Clarmann, T.: Ten years of MIPAS measurements with ESA Level 2 processor V6 – Part 1: Retrieval algorithm and diagnostics of the products, Atmos. Meas. Tech., 6, 2419–2439, doi:10.5194/amt-6-2419-2013, 2013.

Robock, A.: Volcanic eruptions and climate, Rev. Geophys., 38, 191–219, 2000.

Schaefer, J. T.: The critical success index as an indicator of warning skill, Weather Forecast., 5, 570–575, 1990.

Sears, T. M., Thomas, G. E., Carboni, E. A., Smith, A. J., and Grainger, R. G.: SO_2 as a possible proxy for volcanic ash in aviation hazard avoidance, J. Geophys. Res., 118, 5698–5709, 2013.

Seibert, P.: Inverse modelling of sulfur emissions in Europe based on trajectories, in: Volume 114 of Geophysical Monograph, American Geophysical Union, Washington DC, USA, 147–154, 2000.

Solomon, S., Daniel, J. S., Neely, R., Vernier, J.-P., Dutton, E. G., and Thomason, L. W.: The persistently variable "background" stratospheric aerosol layer and global climate change, Science, 333, 866–870, 2011.

Stein, O., Flemming, J., Inness, A., Kaiser, J. W., and Schultz, M. G.: Global reactive gases forecasts and reanalysis in the MACC project, J. Integr. Environ. Sci., 9, 57–70, 2012.

Stohl, A., Forster, C., Frank, A., Seibert, P., and Wotawa, G.: Technical note: The Lagrangian particle dispersion model FLEXPART version 6.2, Atmos. Chem. Phys., 5, 2461–2474, doi:10.5194/acp-5-2461-2005, 2005.

Stohl, A., Prata, A. J., Eckhardt, S., Clarisse, L., Durant, A., Henne, S., Kristiansen, N. I., Minikin, A., Schumann, U., Seibert, P., Stebel, K., Thomas, H. E., Thorsteinsson, T., Tørseth, K., and Weinzierl, B.: Determination of time- and height-resolved volcanic ash emissions and their use for quantitative ash dispersion modeling: the 2010 Eyjafjallajökull eruption, Atmos. Chem. Phys., 11, 4333–4351, doi:10.5194/acp-11-4333-2011, 2011.

Stunder, B. J., Heffter, J. L., and Draxler, R. R.: Airborne volcanic ash forecast area reliability, Weath. Forecast, 122 (5), 1132–1139, 2007.

Theys, N., Campion, R., Clarisse, L., Brenot, H., Gent, J. V., Dils, B., Corradini, S., Merucci, L., Coheur, P.-F., Roozendael, M. V., Hurtmans, D., Clerbaux, C., Tait, S., and Ferrucci, F.: Volcanic SO_2 fluxes derived from satellite data: a survey using OMI, GOME-2, IASI and MODIS, Atmos. Chem. Phys., 13, 5945–5968, doi:10.5194/acp-13-5945-2013, 2013.

Tikhonov, A. N. and Arsenin, V. Y.: Solutions of Ill-posed Problems, V. H. Winston and Sons, Washington, 1977.

Vernier, J.-P., Thomason, L. W., Fairlie, T. D., Minnis, P., Palikonda, R., and Bedka, K. M.: Comment on "Large Volcanic Aerosol Load in the Stratosphere Linked to Asian Monsoon Transport", Science, 339, 647-d, doi:10.1126/science.1227817, 2013.

Webley, P., Stunder, B., and Dean, K.: Preliminary sensitivity study of eruption source parameters for operational volcanic ash cloud transport and dispersion models - a case study of the August 1992 eruption of the Crater Peak vent, Mount Spurr, Alaska, J. Volcanol. Geotherm. Res., 186 (1), 108–119., 2009.

Wernli, H. and Davies, H. C.: A Lagrangian-based analysis of extratropical cyclones, I: The method and some applications, Q. J. Roy. Meteor. Soc., 123, 467–489, 1997.

Winker, D. M., Pelon, J., Coakley, J. A., Ackerman, S. A., Charlson, R. J., Colarco, P. R., Flamant, P., Fu, Q., Hoff, R. M., Kittaka, C., Kubar, T. L., Le Treut, H., McCormick, M. P., Mégie, G., Poole, L., Powell, K., Trepte, C., Vaughan, M. A., and Wielicki, B. A.: The CALIPSO Mission: a global 3D view of aerosols and clouds, B. Am. Meteorol. Soc., 91, 1211–1229, 2010.

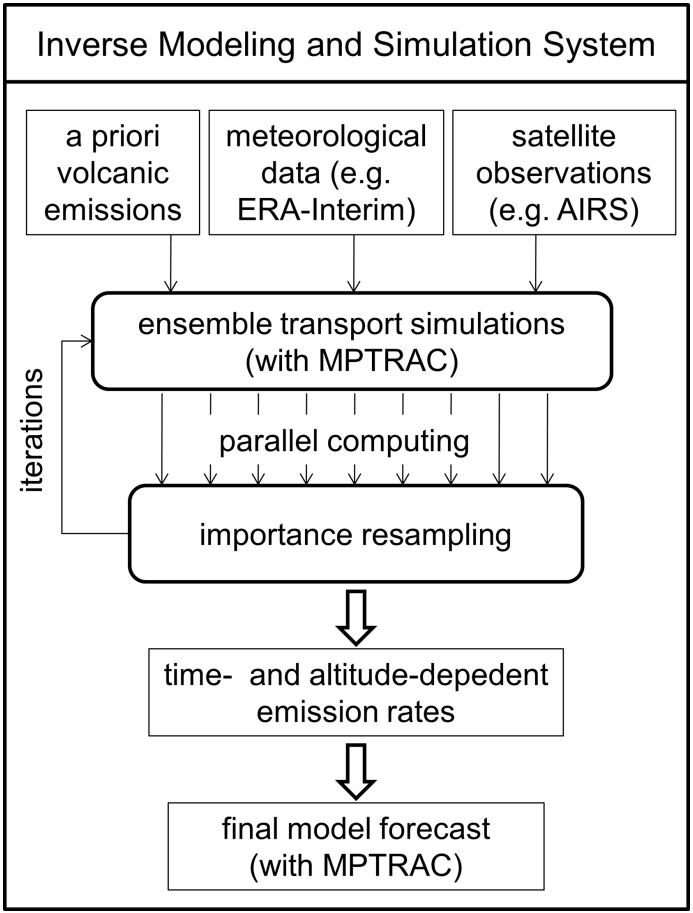

Figure 1. Flow chart of the proposed inverse modeling and simulation system to infer volcanic SO_2 emissions rates and to perform transport simulations.

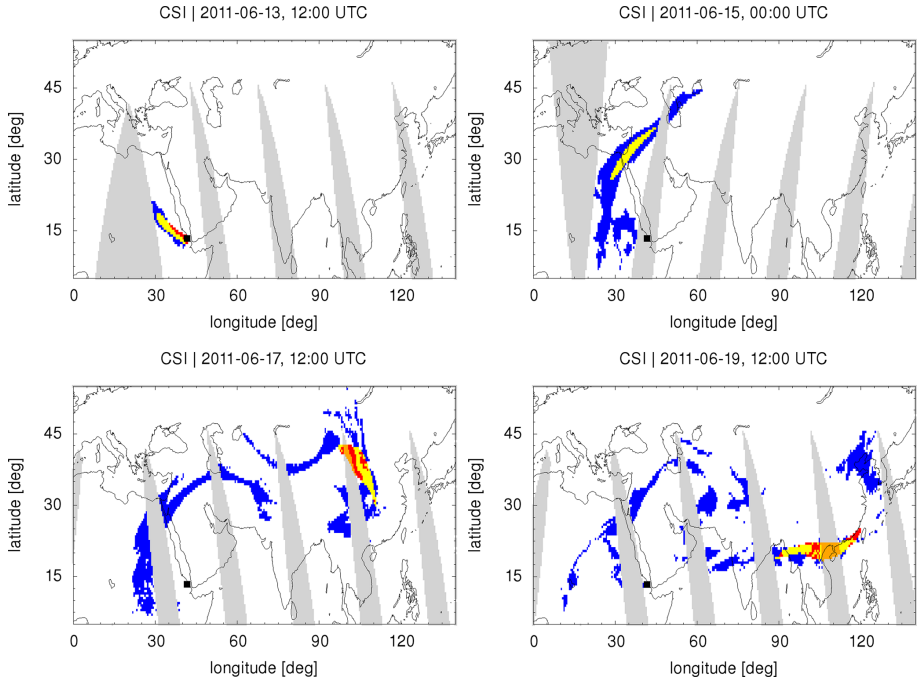

Figure 2. Unit simulation for the Nabro case study with air parcels initialized around 13 June, 00:00 UTC and 16.5 km altitude. The CSI analysis is performed on a $1^\circ \times 1^\circ$ longitude-latitude grid. Gray color indicates missing satellite data. Orange color corresponds to positive model forecasts, but lack of satellite data. Yellow color indicates positive forecasts and positive satellite observations. Blue color corresponds to negative forecasts with positive observations. Red color corresponds to positive forecasts with negative observations. The black square shows the location of the Nabro volcano.

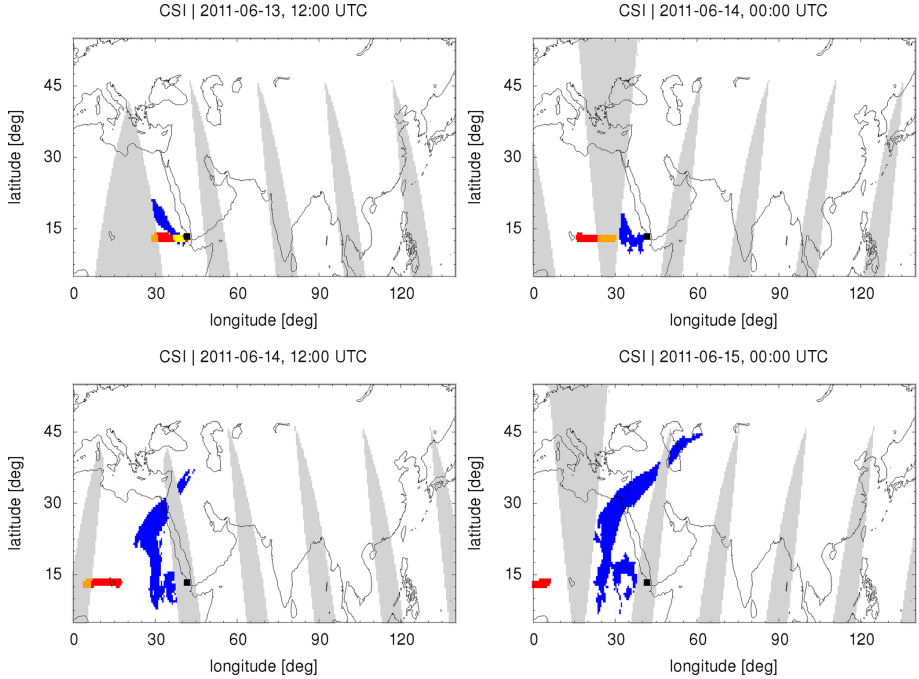

Figure 3. Same as Fig. 2, but for a unit simulation initialized at 29 km altitude. This simulation almost immediately disagrees with the satellite observations. Note that the time steps are partly different from those shown in Fig. 2.

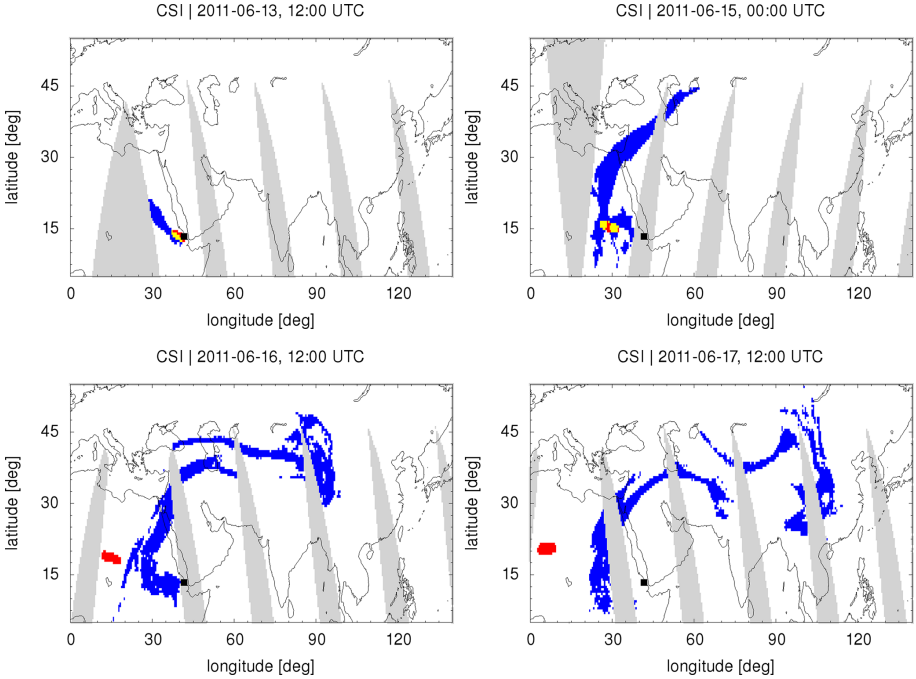

Figure 4. Same as Fig. 2, but for a unit simulation initialized at 20 km altitude. This simulations agrees with the satellite observations for about 48 h, but disagrees at later times. Note that the time steps are partly different from those shown in Figs. 2 and 3.

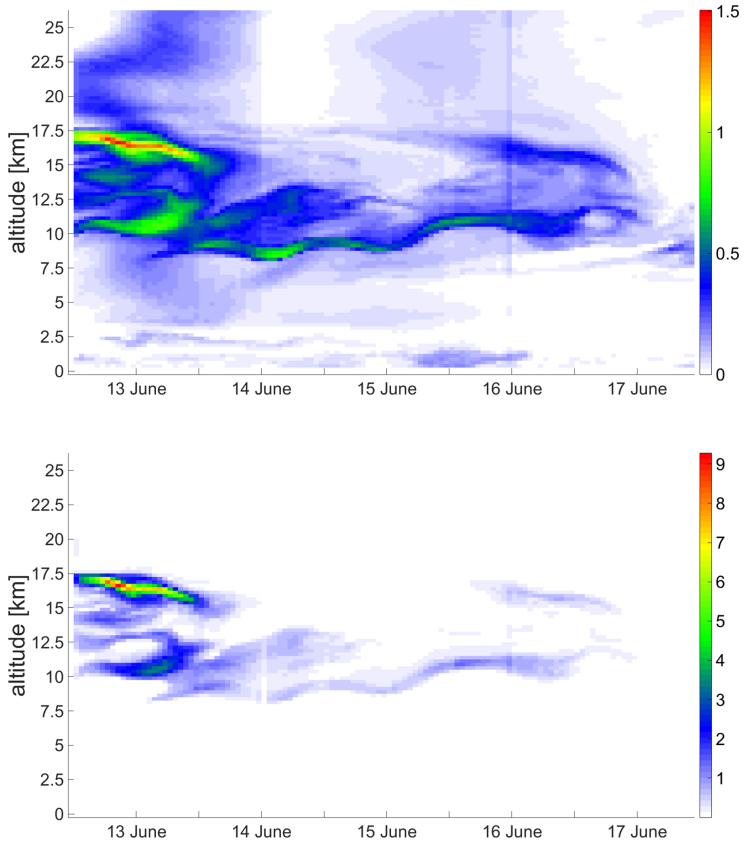

Figure 5. Reconstructed SO_2 emission rates ($kg\,m^{-1}\,s^{-1}$) for the Nabro eruption in June 2011. Emission rates were obtained by applying the mean rule (top) and the product rule (bottom) weight-updating schemes of the proposed inversion approach (see text for details).

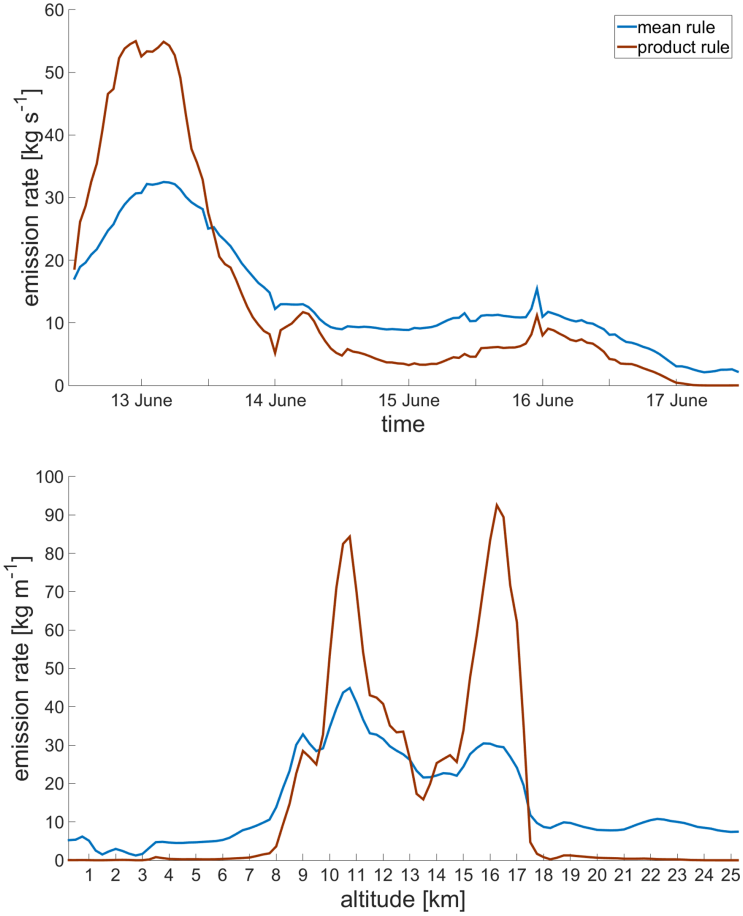

Figure 6. Comparison of reconstructed emission rates integrated over altitude (top) and time (bottom) for the mean rule and the product rule weight-updating schemes.

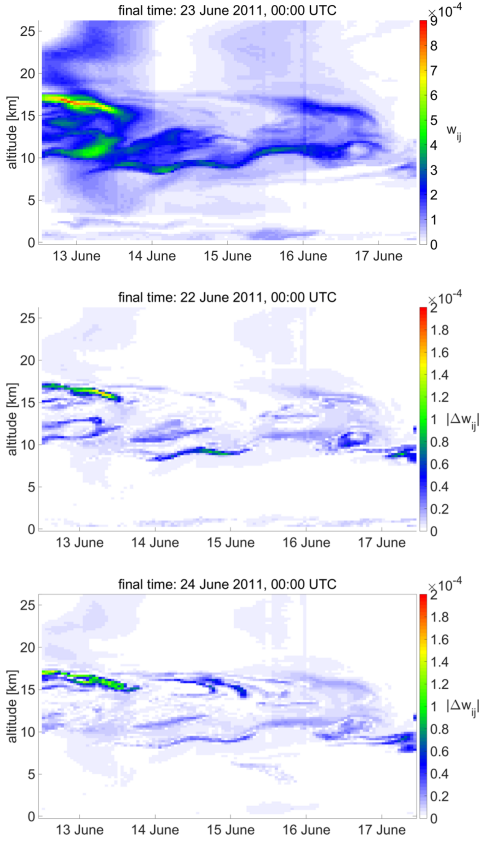

Figure 7. Sensitivity analysis for the mean rule parameter n_k: estimated importance weights w_{ij} for choosing 23 June, 00:00 UTC as the final time of used satellite data (top); absolute differences of estimated importance weights $|\Delta w_{ij}|$ for choosing 23 June, 00:00 UTC as the final time and those for choosing 22 June, 00:00 UTC (middle) and 24 June, 00:00 UTC (bottom) as final time.

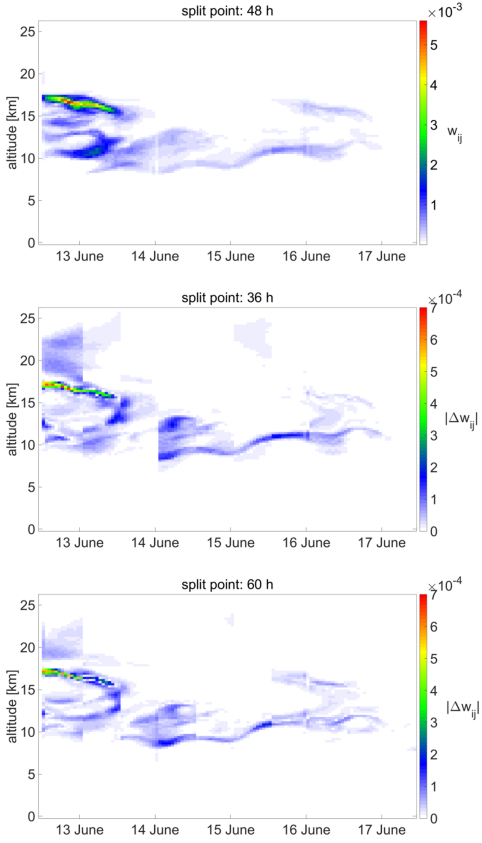

Figure 8. Sensitivity analysis for the product rule parameter n'_k: estimated importance weights w_{ij} for choosing 23 June 00:00 as the final time of used satellite data and 48 h as the split point (top); absolute differences of estimated importance weights $|\Delta w_{ij}|$ for choosing 48 h as the split point and those for choosing 36 h (middle) and 60 h (bottom) as split point.

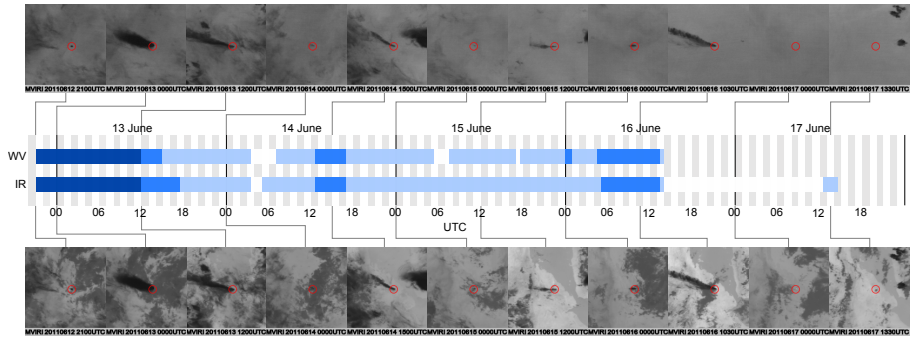

Figure 9. Time line of the 2011 Nabro eruption based on MVIRI IR and WV measurements from Meteosat-7 (IODC). The satellite images were used to roughly estimate the strength of the volcanic activity (white = none, light blue = low level, blue = medium level, dark blue = high level).

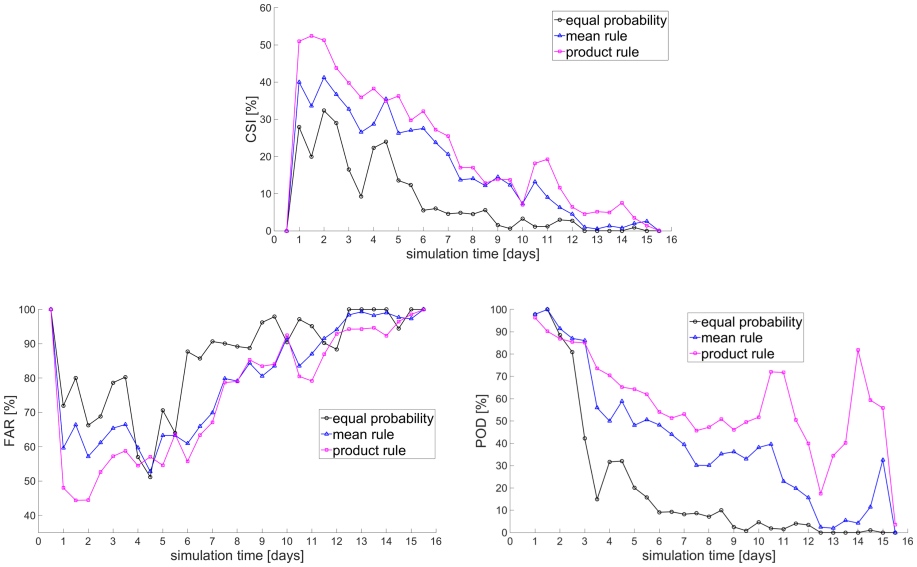

Figure 10. Comparison of the Critical Success Index (CSI), the False Alarm Rate (FAR) and the Probability Of Detection (POD) time series during 12 h time intervals obtained by applying the equal-probability strategy, the mean rule, and the product rule.

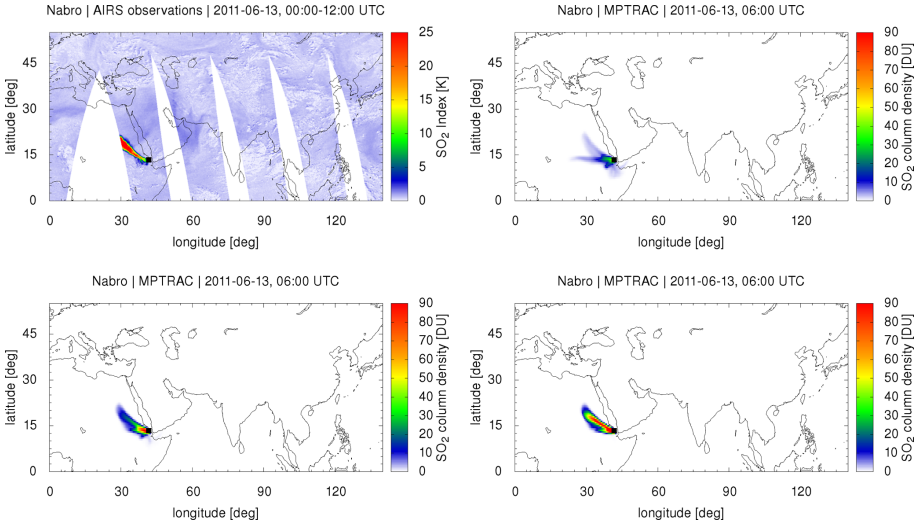

Figure 11. Comparison of AIRS satellite observations (top, left) and MPTRAC simulation results on 13 June 2011, 06:00 UTC based on the equal-probability strategy (top, right), the mean rule (bottom, left), and the product rule (bottom, right).

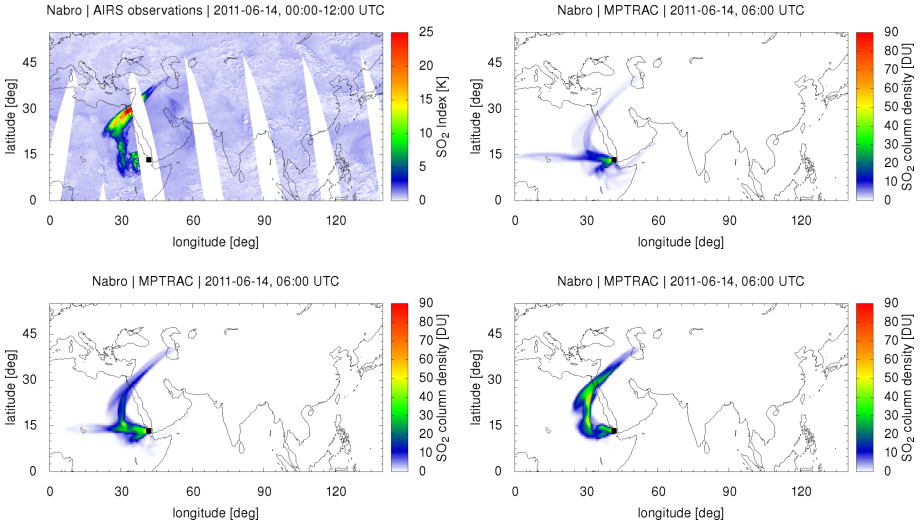

Figure 12. Same as Fig. 11, but for 14 June 2011, 06:00 UTC.

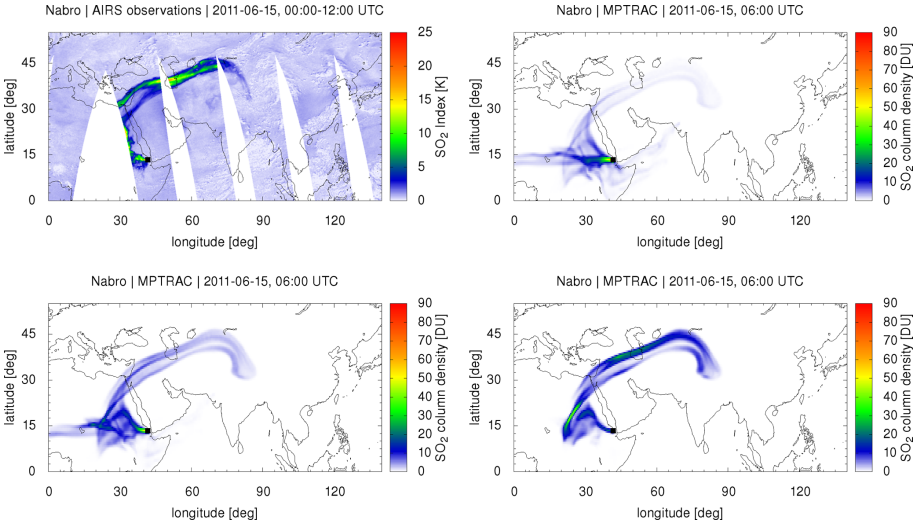

Figure 13. Same as Fig. 11, but for 15 June 2011, 06:00 UTC.

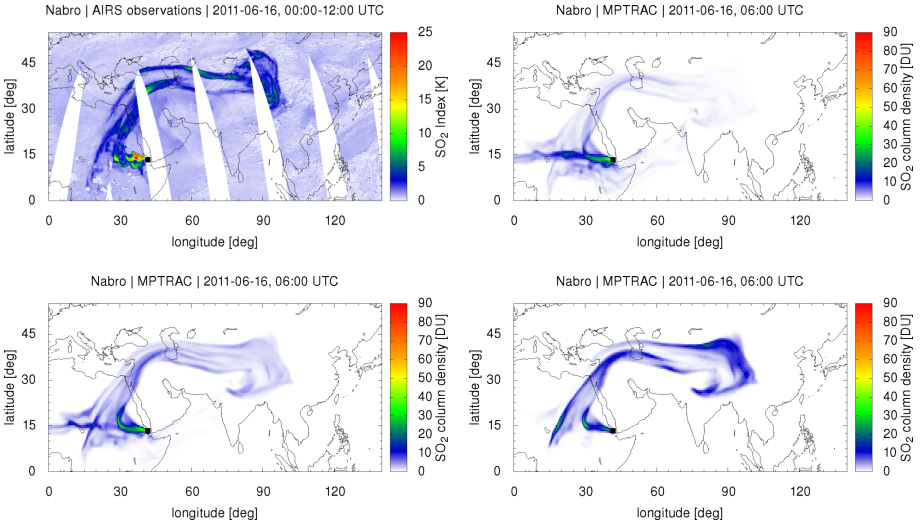

Figure 14. Same as Fig. 11, but for 16 June 2011, 06:00 UTC.

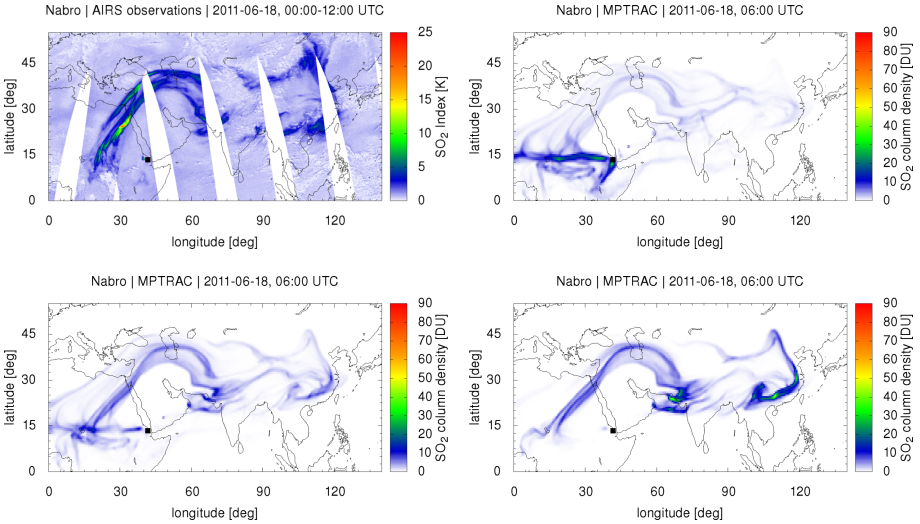

Figure 15. Same as Fig. 11, but for 18 June 2011, 06:00 UTC.

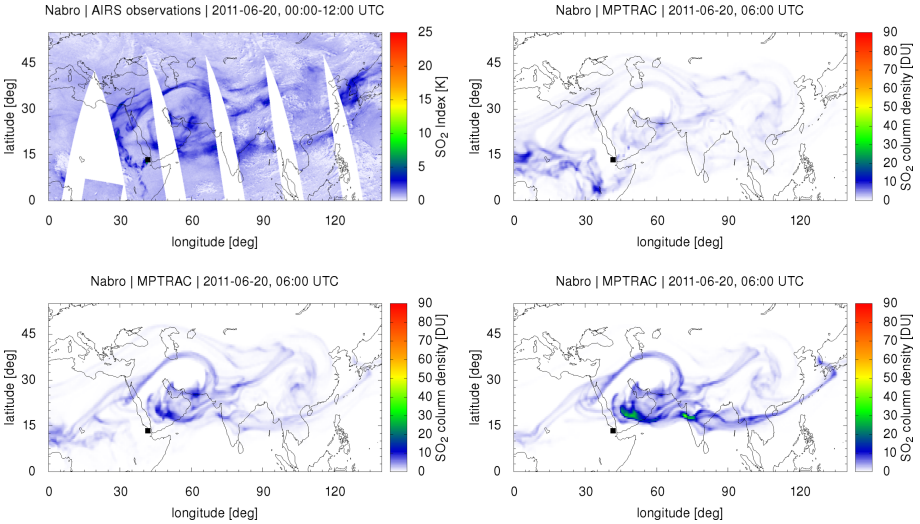

Figure 16. Same as Fig. 11, but for 20 June 2011, 06:00 UTC.

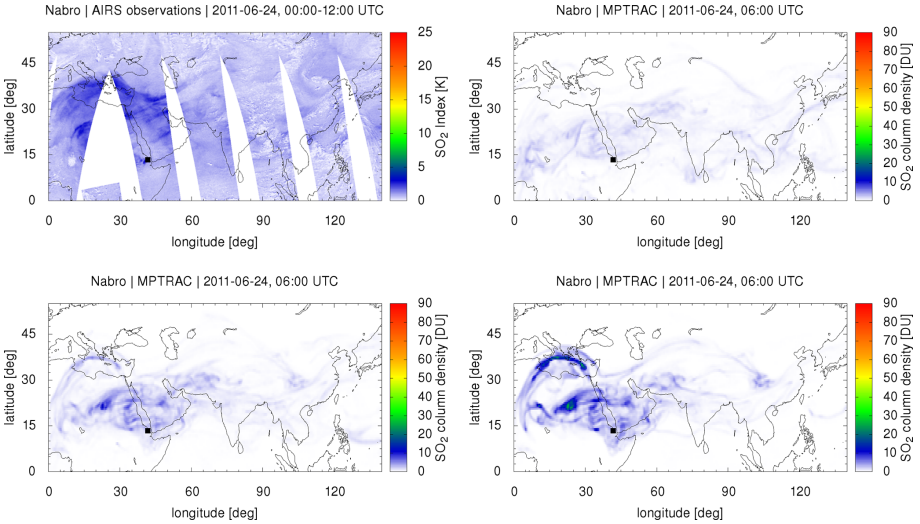

Figure 17. Same as Fig. 11, but for 24 June 2011, 06:00 UTC.

Algorithm 1 Inverse Modeling Approach

Input: time- and altitude-dependent emission domain $E = [t_0, t_f] \times \Omega$, total number and mass of SO_2 air parcels for the final forward simulation, meteorological data, satellite observations

1: Discretize the entire domain E, by considering n_t equal-sized intervals on the time axis and n_h heights along the altitude axis, respectively.

2: Distribute air parcels in all $N = n_t \cdot n_h$ subdomains of E uniformly. Set initial weights according to the equal-probability strategy, $w_{ij} = 1/N$.

3: **Do**

4: Perform N unit simulations in parallel and calculate CSI time series.

5: Update importance weights w_{ij} based on one of the weight-updating schemes described in Sect. 3.3. Resample air parcels distributions according to importance weights.

6: **While** relative difference between adjacent importance weight matrices according to Eq. (7) is larger than a given tolerance.

7: Distribute air parcels in the entire initialization domain based on final importance weights.

8: Perform final forward simulation based on the reconstructed altitude-dependent time series of emissions.

Output: horizontal and vertical trace gas distributions (column densities, lists of air parcels) and diagnostic data (CSI, FAR and POD plots) at different model time steps